CONVECTION EFFECTS IN PROTEIN CRYSTAL GROWTH

Final Report
RAI-87-P-4

Period Covered: 7/28/86 - 6/26/88
Contract: NAS8-36652

Prepared for:
George C. Marshall Space Flight Center
MSFC, AL 35812

Prepared by:
Glyn O. Roberts

Date: 6/26/88

Roberts Associates, Incorporated
1729 Pine Valley Drive
Vienna, VA 22180

Roberts Associates, Incorporated
1726 Pine Valley Drive
Vienna, VA 22180-2341

Tel. (703)938-1757

July 8, 1988

NASA/MSFC
Procurement Office
Code AP29-F

Subject: Final Report on Contract NAS8-36652

Dear Sirs,

We are pleased to present the subject report, approved by the COTR. The attached distribution list is that required by the contract.

Yours sincerely,

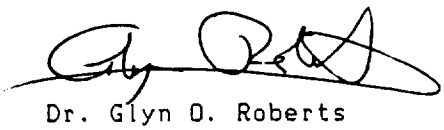

Dr. Glyn O. Roberts
President

Distribution:
AP29-F (0)
CN24D (5)
AT01
CC01/Wofford
EM13A-27/M. Strauss
ES76/Dr. W. Fowlis (2 + repro.)
NASA/STIF (1 + repro.)

TABLE OF CONTENTS

1. INTRODUCTION 1

1.1 Background 1
1.2 Hydrodynamics of Protein Crystal Growth 2
1.3 Model Assumptions 3
1.4 Concentration Boundary Condition 4
1.5 Problem Parameters 5
1.6 Dimensionless Parameters 5
1.7 Dimensionless Equations 6
1.8 Theoretical Estimates 6

2. NUMERICAL METHODS 9

2.1 The AGCE Code 9
2.2 Input Data 9

3. FIXED CONCENTRATION DEFICIENCY 13

3.1 Summary of Cases Computed 13
3.2 Plots of Typical Results 15

4. FIXED GROWTH RATE 28

3.1 Summary of Cases Computed 28
3.2 Plots of Typical Results 30

5. CONCLUSIONS 43

REFERENCES 44

APPENDIX. CONVECTION PROCESSES IN HANGING-DROP CRYSTAL GROWTH 45

A.1 Background 45
A.2 Convection in the Reservoir 45
A.3 Convection in the Vapor Phase 45
A.4 Convection in the Drop 45
A.5 Summary and Illustration 46

LIST OF TABLES

Table 1. Estimates for Dimensional Shear Maximum in Four Limiting Cases 8
Table 2. Summary of Numerical Results for the Fixed-Deficiency Cases 13
Table 3. Summary of Numerical Results for the Fixed Growth Rate Cases 28

LIST OF FIGURES

Figure 1. Observations of Convection from a Growing Crystal. 1
Figure 2. Illustrative Plot of Growth Rate versus Interface Concentration 4
Figure 3. Input Data for the AGCE Code, for a typical case. 10
Figure 4. Logarithmic Plot of the Shear Maximum as a Function of the Rayleigh Number, for the Fixed Deficiency Case. 14
Figure 5. Logarithmic Plot of the Thickness Minimum as a Function of the Rayleigh Number, for the Fixed Deficiency Case. 15
Figure 6. Concentration for Fixed Deficiency Case with S = 1,000 and R = 1 16
Figure 7. Concentration for Fixed Deficiency Case with S = 1,000 and R = 100 17
Figure 8. Concentration for Fixed Deficiency Case with S = 1,000 and R = 10,000 18
Figure 9. Concentration for Fixed Deficiency Case with S = 1,000 and R = 1,000,000 19
Figure 10. Stream Function for Fixed Deficiency Case with S = 1,000 and R = 1 20
Figure 11. Stream Function for Fixed Deficiency Case with S = 1,000 and R = 100 21
Figure 12. Stream Function for Fixed Deficiency Case with S = 1,000 and R = 10,000 22
Figure 13. Stream Function for Fixed Deficiency Case with S = 1,000 and R = 1,000,000 23
Figure 14. Theta Velocity Component for Fixed Deficiency Case with S = 1,000 and R = 1 24
Figure 15. Theta Velocity Component for Fixed Deficiency Case with S = 1,000 and R = 100 25
Figure 16. Theta Velocity Component for Fixed Deficiency Case with S = 1,000 and R = 10,000 26
Figure 17. Theta Velocity Component for Fixed Deficiency Case with S = 1,000 and R = 1,000,000 27
Figure 18. Logarithmic Plot of the Shear Maximum as a Function of the Rayleigh Number, for the Fixed Growth Rate Case. 29
Figure 19. Logarithmic Plot of the Thickness Minimum as a Function of the Rayleigh Number, for the Fixed Growth Rate Case. 30
Figure 20. Concentration for Fixed Growth Rate Case with S = 1,000 and R = 1 31
Figure 21. Concentration for Fixed Growth Rate Case with S = 1,000 and R = 100 32
Figure 22. Concentration for Fixed Growth Rate Case with S = 1,000 and R = 10,000 33
Figure 23. Concentration for Fixed Growth Rate Case with S = 1,000 and R = 1,000,000 34
Figure 24. Stream Function for Fixed Growth Rate Case with S = 1,000 and R = 1 35
Figure 25. Stream Function for Fixed Growth Rate Case

with S = 1,000 and R = 100 36
Figure 26. Stream Function for Fixed Growth Rate Case
with S = 1,000 and R = 10,000 37
Figure 27. Stream Function for Fixed Growth Rate Case
with S = 1,000 and R = 1,000,000 38
Figure 28. Theta Velocity Component for Fixed Growth Rate Case
with S = 1,000 and R = 1 39
Figure 29. Theta Velocity Component for Fixed Growth Rate Case
with S = 1,000 and R = 100 40
Figure 30. Theta Velocity Component for Fixed Growth Rate Case
with S = 1,000 and R = 10,000 41
Figure 31. Theta Velocity Component for Fixed Growth Rate Case
with S = 1,000 and R = 1,000,000 42
Figure 32. Convection Processes in a Hanging Drop Configuration 45

Section 1
INTRODUCTION

1.1 Background

Protein crystals for X-ray diffraction study are usually grown resting on the bottom of a hanging drop of a saturated protein solution, with slow evaporation to the air in a small enclosed cell. The evaporation rate is controlled by hanging the drop above a reservoir of water, with its saturation vapor pressure decreased by a low concentration of a passive solute. The drop has a lower solute concentration, and its volume shrinks by evaporation until the molecular concentrations match.

Protein crystals can also be grown from a seed crystal suspended or supported in the interior of a supersaturated solution. The main analysis of this report concerns this case because it is less complicated than hanging drop growth.

Convection effects have been suggested as the reason for the apparent cessation of growth at a certain rather small crystal size. It seems that as the crystal grows, the number of dislocations increases to a point where further growth is hindered. Growth in the microgravity environment of an orbiting space vehicle has been proposed as a method for obtaining larger crystals.

Experimental observations of convection effects during the growth of protein crystals have been reported by Pusey et al. (1986), Carter (1987), and others. Figure 1 was provided by Pusey.

Figure 1. Observations of Convection from a Growing Crystal.

1.2 Hydrodynamics of Protein Crystal Growth

As a protein crystal grows, the protein concentration in the surrounding supersaturated solution is decreased. This normally also decreases the density, and the fluid rises past the growing crystal and ascends in a buoyant plume.

This convection flow can be expected to produce the following three effects:

It replaces the surrounding fluid with fresh solution from further away.

Growth is asymmetric, since the concentration depletion is least below the crystal, and greatest above it, where the plume leaves.

The shear flow distribution at the crystal boundary modifies the process of crystal growth.

This third effect is of great concern. In quasi-equilibrium, molecules are continually being added to and removed from the crystal, and in the thermal agitation, they can settle in a location of minimum energy, forming a quality crystal. But if the growth occurs in a shear environment, the relative positioning of the added molecules is modified, implying much more dislocations in the added layers of crystal. It has been suggested by many workers that the accumulation of these dislocations may impede further crystal growth.

If there is ambient density stratification, due to temperature gradients or to concentration gradients produced by the crystal growth or maintained externally, the convection flow is modified. In the simplest cases, the ambient supersaturated fluid at a distance from the crystal can be regarded as homogeneous.

There are other hydrodynamic phenomena and issues in hanging-drop protein crystal growth.

One issue is the shape of the hanging drop, and the limits on its size. With appropriate support, much larger drops can be used in a microgravity environment. The water reservoir must also be supported, of course, for example it can be held by surface tension in a porous material.

A second hydrodynamic issue is the transport of evaporated moisture away from the drop, by a combination of diffusion and free or forced convection.

The processes of evaporation and condensation lead to density variations in the drop and reservoir. The variation of the solute concentration in the reservoir, and of the solute and protein concentration in the drop, is controlled by diffusion and convection processes.

A fourth issue is capillary convection in the drop, with surface tension variations caused by variations in the temperature and concentration.

These phenomena are discussed further in the appendix. Their detailed study is beyond the scope of this present analysis. Attention is confined in

the rest of this report to the growth of a supported crystal in an large fluid volume.

1.3 Model Assumptions

We have performed numerical computations of the total flow and concentration distributions, including the boundary layer thicknesses and boundary shear flow, in the convection near a growing spherical crystal. We made the following assumptions:

the growing crystal remains spherical;

its growth rate is negligible compared with the convection flow speeds in the surrounding solution;

the surrounding fluid volume is effectively infinite, and the fluid at large distances is homogeneous (except in the ascending buoyant plume);

temperature variations are negligible;

effects of the 'sting' support for the crystal are neglected.

The limitations of these assumptions are discussed in the following paragraphs.

The protein crystal will not be spherical. New molecules prefer to add themselves to an existing layer, rather than to start a new layer. The crystal shapes formed are therefore particular to the individual molecule. In addition, the convection flow may establish preferred directions of growth, because of variations in flux around the surface and because of velocity shear on the sides. This assumption of a spherical shape will of course be better for some proteins than for others.

The growth rate of the crystal, relative to the flow speeds, depends on a number of parameters, including the degree of supersaturation of the fluid, the protein concentration in the crystal (rarely 100%), and the Rayleigh number (discussed below). This assumption is generally a good one.

The surrounding fluid is effectively infinite if its dimensions are at least thirty to a hundred times the crystal radius. The requirements obviously depend on the accuracy required. The boundaries modify the flow, and the concentration depletion in the plume collects at the top of the chamber and spreads downward.

Temperature effects are negligible because little heat is generated in protein crystallization and because the diffusivity for heat is so much more than for protein concentration. External temperature effects, and resulting convection, may be important in some configurations.

The support for the crystal will cause minimal flow modification if it is a thin 'sting' with the crystal on the end, and if it extends up vertically from the bottom of the chamber. A side sting support will cause a larger flow modification.

1.4 Concentration Boundary Condition

We consider two limiting cases for the concentration boundary condition on the crystal surface. In the first limit, the concentration deficiency (compared with the supersaturated protein solution at infinity) at the crystal surface is fixed, while the growth rate varies with position depending on the calculated flux of protein toward the surface. In the second limit, the growth rate and flux are fixed, while the concentration deficiency varies over the crystal surface. Numerical results are presented for both cases.

The truth is between these two limits, as illustrated below. The figure shows the protein flux (linearly equivalent to the growth rate or to the normal derivative of the concentration) as a linear function of the excess concentration at the interface over saturation. Note that equilibrium at the interface is only a good approximation if growth is extremely slow, because of the large size of the protein molecules of interest.

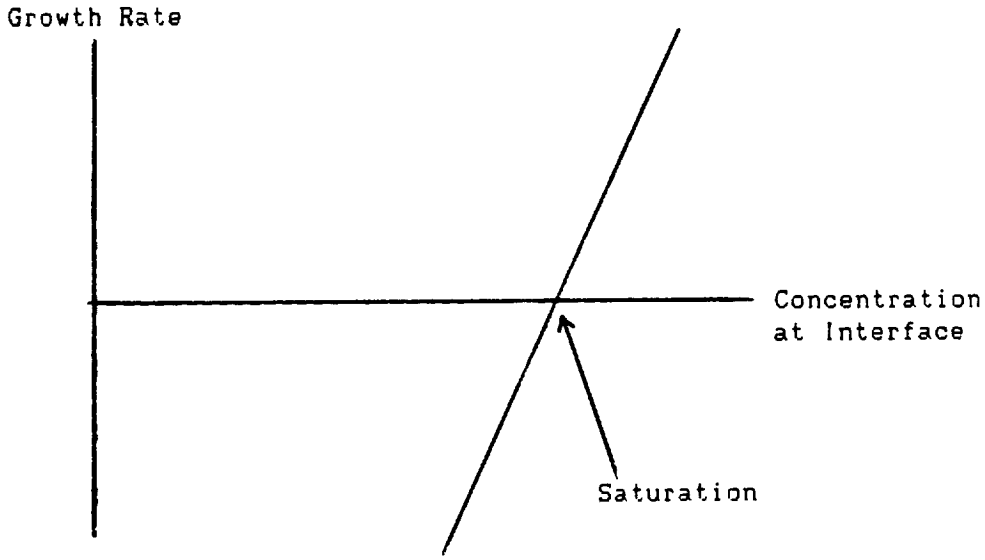

Figure 2. Illustrative Plot of Growth Rate versus Interface Concentration

In the first limit, the supersaturation at the interface is small compared with that at large distances, so that the interface deficiency is effectively constant. In the second limit, the supersaturation at the interface is only very slightly less than the supersaturation at infinity, so that the flux is effectively constant. Plainly, the truth will always be somewhere between these two extremes.

We have not included any reduction in the growth rate due to interface velocity shear, in our model computations. We have merely computed the shear as a function of the radius and the other parameters. It is our hypothesis that as the radius increases, the corresponding increase in shear velocity modifies the growth process, leading to an increasing number of dislocations. Further growth is stopped, since the supersaturation of the fluid cannot be increased further without spontaneous nucleation.

1.5 Problem Parameters

The key constant parameters defining the problem are as follows:

crystal radius a;

gravity g;

mean density ρ;

kinematic viscosity ν; and

diffusivity for the protein, D; and either

surface relative density deficiency C for protein concentration; or

surface relative density gradient C' for the second limit.

Values of interest are as follows:

$a < 0.1$ cm,

$g = 980$ cm/sec^2 (or about 0.01 cm/sec^2 for microgravity),

$\rho = 1$ gm/cc,

$\nu = 0.01$ cm^2/sec,

$D = 10^{-7}$ to 10^{-5} cm^2/sec, and either

$C < 0.0001$ (no units), for the first limit, or

$C' < 0.001$ cm^{-1}, for the second limit.

1.6 Dimensionless Parameters

From these input parameters, we can derive two independent dimensionless parameters characterizing the flow. The Schmidt number is

$$S = \nu/D = 10^3 \text{ to } 10^5.$$

The Rayleigh number is

$$R = \frac{gCa^3}{\nu D},$$

for the first limit, and

$$R = \frac{gC'a^4}{\nu D},$$

for the second. The Grasshof number R/S is also in common use. Using the parameter ranges above, its maximum possible value is unity, corresponding to R values up to about 10^5.

1.7 Dimensionless Equations

Using the length scale a and the diffusivity scale D yields the dimensionless equations

$$S^{-1}\frac{Du}{Dt} = -\nabla p + \nabla^2 \underline{u} + Rc\hat{z} ,$$

$$\frac{Dc}{Dt} = \nabla^2 c .$$

The flow $\underline{u}$ is zero on the spherical boundary r = 1. The variables tend to zero at infinity. The dimensionless concentration c is unity on r = 1, in the first limit where the value is imposed on the growing crystal surface. In the other limit of imposing a fixed flux, the boundary condition is

$$\partial c/\partial r = -1 .$$

To obtain the dimensional variables from the corresponding dimensionless variables, they must be multiplied by the following scales:

length a (cm);

speed D/a (cm/sec);

time a^2/D (sec);

pressure $\rho D/a^2$ (dynes/cm^2); and

relative density deficiency C or C'a (no units).

1.8 Theoretical Estimates

This system of equations is not amenable to analytic solution, and must be solved numerically. The scales of the solution can be estimated, and this is an important preliminary to numerical solution.

In the first place, the momentum term in the equation of motion is always small in comparison with the viscous term, since S is so large.

For R small compared with 1, the concentration solution near the sphere is approximated by the conduction (no flow) solution c = 1/r. This applies in both limiting cases, with the boundary condition c = 1 or with the boundary condition that the radial derivative is -1. The equation of motion determines the dimensionless flow speed magnitude as a function of radius, as of order

$$R(r-1).$$

The corresponding shear on the crystal boundary is of order R. The upper limit on the radius, for the conduction solution and the corresponding flow solution to apply, is

$$r < R^{-1/2}.$$

The theoretical estimates for the dimensionless flow and boundary layer thickness, for large R, are more difficult. Assume boundary layer thickness T and velocity shear Q. Then the velocity in the layer is QT. From the concentration equation balance,

$$QT = 1/T^2.$$

Also the ratio of the concentration deficiency (compared with infinity) to its normal derivative at the interface is T (whichever of these two quantities is imposed by the boundary condition). Assuming that the buoyancy in the layer is significant in driving the shear (rather than the shear being mostly due to plume buoyancy), the motion balance gives in the two limits,

$$QT/T^2 = R, \text{ and}$$

$$QT/T^2 = RT.$$

Thus, when the concentration deficiency as compared with infinity is imposed, the shear and thickness are of order

$$Q = R^{3/4},$$

$$T = R^{-1/4},$$

while when the concentration deficiency gradient is imposed, the shear and thickness are of order

$$Q = R^{3/5},$$

$$T = R^{-1/5}.$$

The numerical results confirm these estimates.

The plume thickness, as the buoyant plume leaves the crystal, is of the same order. The angular thickness decreases without limit as the plume rises and its speed increases, so that full resolution of the whole plume using a spherical polar mesh is impossible. Fortunately, accurate resolution of the far plume and of the far-field flow which it drives is not a requirement, in the study of convection effects on protein crystal growth.

The dimensional shear is QD/a^2. Substituting our three formulae for Q,

$$Q = R, \quad \text{for } R \ll 1,$$

$$Q = R^{3/4}, \quad \text{for } R \gg 1, \text{ fixed deficiency},$$

$$Q = R^{3/5}, \quad \text{for } R \gg 1, \text{ fixed growth rate},$$

and using our two definitions of R and its dependence on a, gives

$$\text{Dimensional shear} \sim a^b,$$

where

$$b = 1, \quad \text{for } R \ll 1, \text{ fixed deficiency},$$

$$b = 2, \quad \text{for } R \ll 1, \text{ fixed growth rate},$$

$$b = 1/4, \quad \text{for } R \gg 1, \text{ fixed deficiency},$$

$$b = 2/5, \quad \text{for } R \gg 1, \text{ fixed growth rate}.$$

More precisely, we can derive the following table for the dimensional shear in the limits of small and large R, for fixed deficiency and for fixed growth rate.

	Fixed Deficiency	Fixed Growth Rate
$R \ll 1$	$\frac{gCa}{\nu}$	$\frac{gCa^2}{\nu}$
$R \gg 1$	$(gC/R\nu)^{3/4}(Da)^{1/4}$	$(gC'/D\nu)^{3/5}(Da)^{2/5}$

Table 1. Estimates for Dimensional Shear Maximum in Four Limiting Cases

Section 2
NUMERICAL METHODS

2.1 Convection Modelling with the AGCE Code

We have modeled convection effects in protein crystal growth by using an existing computer code. This flexible code was developed by the present author, under MSFC sponsorship, to model thermal convection in a spherical layer. The design objective for the code was studies related to NASA's proposed Atmospheric General Circulation Experiment (AGCE). The code was built with great flexibility, and with minor modifications and appropriately chosen input data it was well suited to NASA's requirements in this study.

The code uses the primitive variables in spherical polar coordinates. The vorticity-stream function formulation was avoided, to facilitate the use of the code for stability analyses and in three dimensions. The domain is rectangular in these coordinates, which allows for the whole region between an inner and outer sphere. A wide range of options is available for the thermal boundary conditions on each boundary segment. With the substitution of concentration for temperature, the code was ready for use with almost no other changes. We imposed zero dimensionless density deficiency (scaled concentration deficiency) on a large outer radius (which is a good approximation as discussed in Section 1.3). On the inner sphere of radius unity, we imposed one of the two limiting dimensionless concentration boundary conditions.

Th code allows the use of flexibly-defined non-uniform meshes. These allowed us to resolve the thin boundary layers on the sphere (for large R), without wasting mesh points on the regions far from the sphere. Similarly, we could resolve the thermal plume (at least near the crystal) without using a fine θ mesh outside the plume.

The numerical method options available in the AGCE code include iteration to a steady state using an algorithm which approximates time-stepping the unsteady equations, but with a time step which varies with position. This was a crucial factor in obtaining steady-state solutions in reasonable time, and at reasonable cost in computer resources, since the time scales vary enormously in this application over the relevant domain. Implicit algorithms are used for the advection and diffusion of heat and momentum, and for the representation of internal gravity waves.

2.2 Input Data

Sample data for the AGCE computer code for this application is shown below. The input parameters are divided into three groups, concerned with the problem, the numerical method, and the output. The problem is for the imposed concentration deficiency case, with S = 1000 and R = 10,000, as indicated in the top line.

The data reflects the non-dimensional problem, even though the code accepts dimensional data.

```
CRYSTAL/S=1000/R=10000                    ***PROBLEM PARAMETERS***

DOMAIN                BOUNDARY LAYER      DIFFUSIVITIES          BUOYANCY FORCE          INTERIOR HEATING
BOUNDARIES            THICKNESS FOR MESH  ROTATION RATES         SURFTC=      .0000000   POWERS OF TH & R
THL =      .0000000   DTHL =      .0400000  ANU    = 1000.0000000  GTERR =  1000.0000000  AIHEAT =    .0000000
THR =     3.1415926   DTHR =     1.0000000  AKAPPA =    1.0000000  GDIEL =      .0000000  PIHTTH =    .0000000
RB  =     1.0000000   DRB  =      .0800000  OMEGAC =     .0000000  PDIEL =      .0000000  PIHTR  =    .0000000
RT  =    30.0000000   DRT  =    30.1000000  OMEGAM =     .0000000  ALPHA = 10000.0000000  CIHTTH =    .0000000
PORR=      .0000000   PORTH=      .0000000  OMEGAI =     .0000000  ALPHA2=      .0000000  CIHTR  =    .0000000
ZONAL WAVE NUMBER RANGE =   5,   5,   1

BOUNDARY TEMPERATURE  SIDE & CORNER   BOUNDARY TEMPERATURE INTERPOLATION     BOUNDARY VELOCITY
1 - VALUE FIXED       TEMPERATURES    LINEAR IN TH**IT OR R**IT             1 - NO - SLIP     4 - STRESS/SLIP = OM
2 - ZERO FLUX  4 - FIXED, <ALTH,ALR   IT = -9 & 99 FOR INFINITY             2 - FREE - SLIP
3 - AXIS       5 - FIXED, >ALTH,ALR   ALTH =  .5000000  ALR =    6.0000000  3 - AXIS
LTBOT  = 1  ABOT  =  .00  TTL =  .00  ITBOT  = 1 -3:COS(TH/ALTH)             LUBOT  = 1        OMBOT  =     .0000000
LTTOP  = 1  ATOP  =  .00  TTR =  .00  ITTOP  = 1 -4:LOG(TAN4(TH/2)+T4(A/2))  LUTOP  = 1        OMTOP  =     .0000000
LTLEFT = 3  ALEFT =  .00  TBL = 1.00  ITLEFT = 1                            LULEFT = 3        OMLEFT =     .0000000
LTRITE = 3  ARITE =  .00  TBR = 1.00  ITRITE = 1                            LURITE = 3        OMRITE =     .0000000

                                      ***METHOD PARAMETERS***

NUMBER OF STEPS       TEMPERATURE TIME STEP   VELOCITY TIME STEP     UPWIND DIFFERENCES     REQUIRED CONVERGENCE
NSTEP  = 6127         TAUT =  0.010           TAUU =  .00003         TUPWND =    .100       RCONV  =  9.000
INITIAL TEMPERATURE   PTTH =  1.000           PUTH =  1.000          UUPWND =    .100       DCEVM  =  1.000
TINIT  =     .00      PTR  =  1.000           PUR  =  1.000          SMTHU  =    .000       SMTHW  =   .000

 IMPLICIT AMPLITUDES AND CONTROLS      IMPLICIT AMPLITUDES AND CONTROLS      PRESSURE METHOD
BETTA  =  .60          FIXTTH = T     BETTD  =  .60          FIXTR  = T     NPITER =  7
BETUA  =  .60          FIXUTH = T     BETUD  =  .60          FIXUR  = T     PEXTRP = 1.00
BETUC  = 1.00          FIXUC  = T     BETINT = 1.00          FIXINT = T   ADINT = 0.20

                                      ***OUTPUT PARAMETERS***

CONCENTRATION        C
DIRECT ACCESS READ & WRITE SEGMENTS      WRITE STEP BEGINNING & INCREMENT     DIAGNOSTIC FREQUENCY   CONTOUR LINES
ISEGR =   1  ISEGW =   1  ISEGS =   1      IBEGDA =  0    IINCDA = 900          NDIAG = 0     NCLP = 0  NCLI = 0
(0: ANALYTIC. -1: AFTER PRIOR CASE)        (ZERO MEANS NSTEP)                   RTOP =  4.00              NCOPYS = 1
        ISTEP BEGIN & INCREMENT FOR PRINTER DIAGNOSTICS      RANGES FOR I AND K      PLOTTER IDAOUT BEGIN & INCREMENT
VARIABLE  PHYSICAL CONTOUR  INTEGER CONTOUR  PRINT NUMBERS   IB  IE  II   KB  KE  KI     PHYSICAL      INTEGER      INCR
   U        9901  9902       9903  9904      9905  9906      1  22   1    22   1  -1       1  9914    9915  9001     .0
   V        9901  9902       9903  9904      9905  9906      1  22   1    22   1  -1    9913  9914    9915  9916     .0
   W        9901  9902       9903  9904      9905  9906      1  22   1    22   1  -1    9913  9914    9915  9916     .0
   T        6127  9902       6127  9904      9905  9906      1  22   1    22   1  -1       1  9914    9915  9001     .0
   P        9901  9902       9903  9904      9905  9906      1  22   1    22   1  -1    9913  9914    9915  9916     .0
   DP       9901  9902       9903  9904      9905  9906      1  22   1    22   1  -1    9913  9914    9915  9916     .0
   DU       8901  9902       6127  9904      9905  9906      1  22   1    22   1  -1    9913  9914    9915  9916     .0
   DV       9901  9902       9903  9904      9905  9906      1  22   1    22   1  -1    9913  9914    9915  9916     .0
   DW       8901  9902       6127  9904      9905  9906      1  22   1    22   1  -1    9913  9914    9915  9916     .0
   DT       8901  9902       6127  9904      9905  9906      1  22   1    22   1  -1    9913  9914    9915  9916     .0
   PSI      6127  9902       9903  9904      9905  9906      1  21   1    21   1  -1       1  9914    9915  9916     .0
   VORT     9901  9902       9903  9904      9905  9906      1  21   1    21   1  -1    9913  9914    9915  9916     .0
   AAM      9901  9902       9903  9904      9905  9906      1  22   1    22   1  -1    9913  9914    9915  9916     .0
   OMEG     9901  9902       9903  9904      9905  9906      1  22   1    22   1  -1    9913  9914    9915  9916     .0
   ****     9901  9902       9903  9904      9905  9906      1  22   1    22   1  -1    9913  9914    9915  9916     .0
```

Figure 3. Input Data for the AGCE Code, for a typical case.

The left and right θ boundaries THL and THR are of course zero and π, corresponding to the upward and downward axes. The inner radius RB is unity. The outer radius RB of the computational domain is an approximation to an infinite domain; the results should be unaffected by any larger choice. This was confirmed using an outer radius of 50.

The viscosity ANU and the thermal diffusivity AKAPPA are S (1000 in this case) and unity. The constants ALPHA and GTERR multiply the temperature to give the upward buoyancy acceleration; we therefore always set GTERR to S and ALPHA to R. Thus the equation of motion is precisely that in Section 1.7, multiplied through by S.

The code uses nonuniform computational meshes in the radial and theta directions. The radial mesh spacing is proportional to the product

$$(RT + DRT - r)(r - RB + DRB).$$

A similar expression defines the theta mesh, using DTHL and DTHR. The quantities DRB and DTHL are small, to give adequate resolution of the boundary layer on the sphere and of the rising plume.

The LTxxx variables establish that the "temperature" c is imposed on the "bottom" RB and on the "top" RT, while axis boundary conditions are applied on the axis ("left" and "right"). The corner temperatures (TTL means "temperature top left") determine the imposed temperatures on the top and bottom boundaries as zero and unity, independent of the interpolation method. The velocity boundary conditions are no-slip (zero) at the top and bottom, and normal axis conditions at the axis boundaries.

The OMxxx quantities are rotation rates, and are of course not applicable here. The same applies to other zero problem parameters.

The first group of method parameters define and control the iteration method, with the number NSTEP of iterations, the nominal time steps TAUT and TAUU which are used for temperature and velocity at the coarsest part of the mesh, and the powers of the mesh spacings in the two directions (PTTH, PTR, PUTH, and PUR), used to decrease these nominal time steps. The time steps are very small in the plume and in the boundary layer on the inner sphere. The upwind differencing parameters introduce a very small amount of upwind differencing in the representations of the temperature and velocity equations, only for cases and at mesh points where it is needed, to avoid mesh separation. Otherwise accurate central differences are used in the representation of all terms.

The second group of method parameters define and control the implicit computation. Implicit methods are required because of the thin layers, high speeds, and convergence requirements. The logical FIXxx variables are T (true), indicating that implicit methods are used in both coordinate directions for both temperature and velocity, and also for internal waves. The BETxx variables determine the precise form of the implicit methods used, and values between a half and unity are appropriate.

The first group of output parameters describe the restart options. When ISEGR is zero, the computation is begun from analytic initial conditions defined by the problem parameters. Complete data for a restart are written to a direct access file every IINCDA steps, beginning with segment ISEGW at step IBEGDA (for which zero indicates NSTEP as in this data). With ISEGR equal to

1, as in this case, the initial conditions are read in from the previously-written segment 1 of the direct access file.

The remaining output parameters control the printed and plotted output. The variable RTOP is the outer radius for plots, and is of course much less than the variable RT. Printer graphics and numerical output are produced from the run itself, for the indicate variables, beginning at the indicated steps (iterations) and at the indicated frequency. For this data, the temperature T and the stream function PSI are plotted on the printer at iteration 6127, which is the last iteration. The temperature and the changes in the velocity components and temperature are also plotted against the integers, as a measure of resolution and convergence.

The quality plots are produced in a separate computation which uses the direct access file for input, and reads this same input data. With this data, U, T and PSI are plotted, from the data on segment 1 of the direct access file.

Section 3
FIXED CONCENTRATION DEFICIENCY

3.1 Summary of Cases Computed

Table 2 is a summary of the fixed-deficiency cases which we have computed. For S equal to 1000, we did R values increasing by factors of ten from one to a million. In addition, we did R values of 1, 1,000, and 100,000, with S equal to 100,000. In each case, the table shows two sets of results, obtained using a 40x40 mesh and using an 80x80 mesh (labeled LOW and HIGH RESOLUTION respectively, to indicate the resolution). For each case and resolution, three numerical values are shown:

the maximum shear $Q = \partial u_\theta / \partial r$, on the interface; and

the maximum and minimum normal derivative of the concentration $\partial c / \partial r$.

In each case, the negative sign is dropped.

		LOW RESOLUTION			HIGH RESOLUTION		
S	R	SHEAR	$\partial c/\partial r_{max}$	$\partial c/\partial r_{min}$	SHEAR	$\partial c/\partial r_{max}$	$\partial c/\partial r_{min}$
1,000	1	3.07	1.491	0.959	3.41	1.542	0.974
	10	14.46	1.997	0.923	19.86	2.155	0.922
	100	66.88	2.827	0.860	70.07	2.874	0.870
	1,000	320.20	4.413	0.790	336.45	4.417	0.810
	10,000	1539.10	7.565	0.703	1642.20	7.244	0.766
	100,000	7348.10	13.628	0.579	8083.30	12.726	0.714
	1,000,000	33187.00	20.191	0.216	39799.00	23.922	0.622
100,000	1	3.07	1.491	0.959	3.13	1.501	0.964
	1,000	322.44	4.416	0.791	332.41	4.360	0.811
	100,000	7609.10	13.634	0.581	8695.70	13.868	0.764

Table 2. Summary of Numerical Results for the Fixed-Deficiency Cases

The following points should be noted about these results.

First, the error of the high-resolution case is less than a quarter of the error of the low resolution case, because the method parameters and the domain choice RB were improved in each case for the high-resolution run, based on the low-resolution results. Comparing the numbers, it can be seen that all the high resolution results have satisfactory accuracy.

Secondly, the differences between the results for the two different values of S are very small. For this reason, we did not do an exhaustive analysis of the effect of S. This result is consistent with the analysis in Section 1.8; since S enters the equations only in the momentum term, which is multiplied by the reciprocal of S.

Thirdly, the minimum of the concentration derivative occurs at the end of the plume, and is of relatively little significance. The maximum of the normal derivative of the concentration is a measure of the reciprocal of the boundary layer thickness, since the interface concentration is unity.

Fourthly, the boundary layer thickness becomes very small as R increase, as predicted theoretically in Section 1.8. For this reason, the input data used decreasing values of the parameters DRB and DTHL (cf. Section 2.2) as R increased, in order to resolve the boundary layer and plume.

Figure 4 is a logarithmic plot of the maximum shear on the interface, as a function of the Rayleigh number R. The slope at large R is close to the predicted value of 3/4. We did not go to small enough R to obtain the predicted slope in that region of unity.

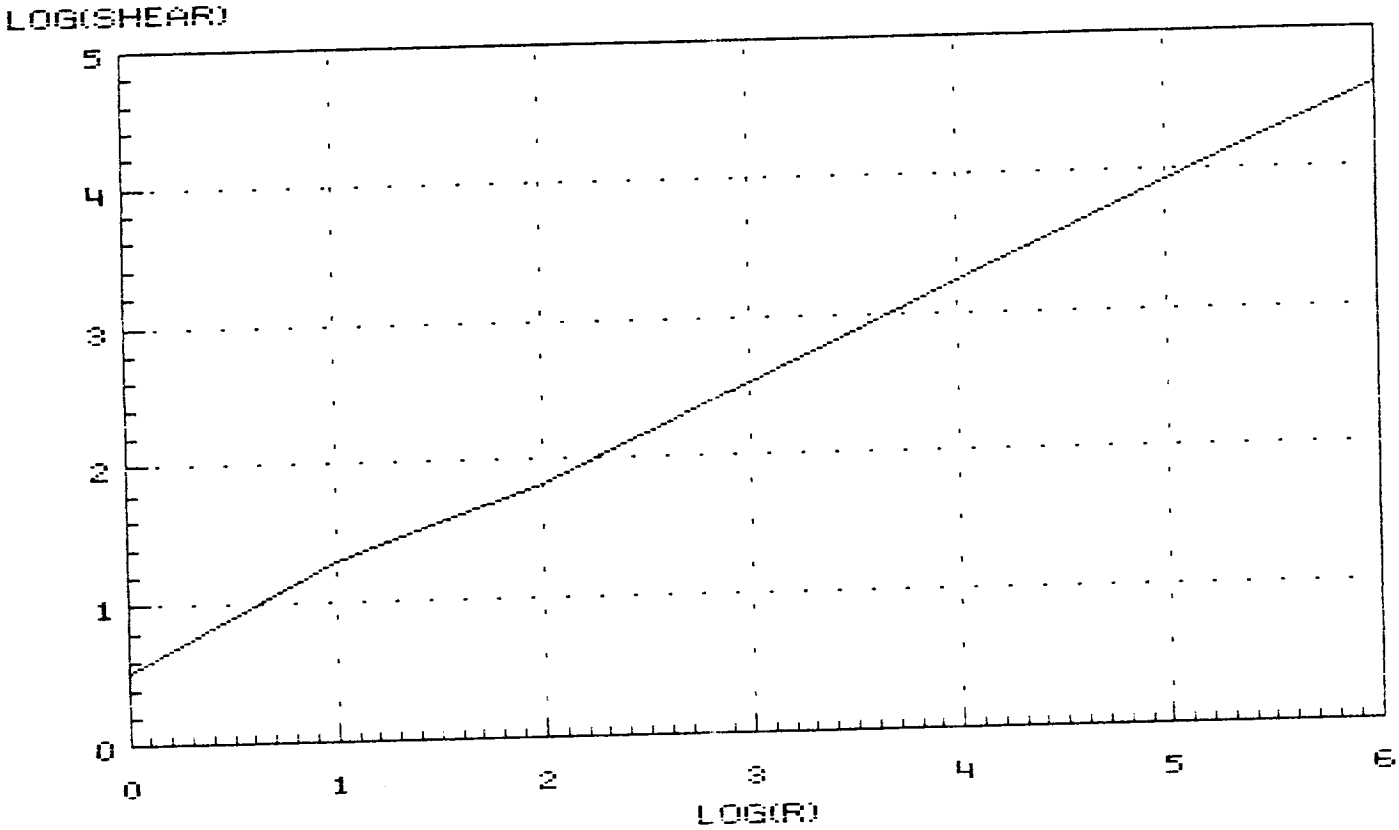

Figure 4. Logarithmic Plot of the Shear Maximum as a Function of the Rayleigh Number, for the Fixed Deficiency Case.

Figure 5 is a logarithmic plot of the boundary layer thickness as a function of R. Again, the slope is close to the predicted value of 1/4, for large R. For small R, the analytic solution T = 1/r is approached, with constant thickness unity.

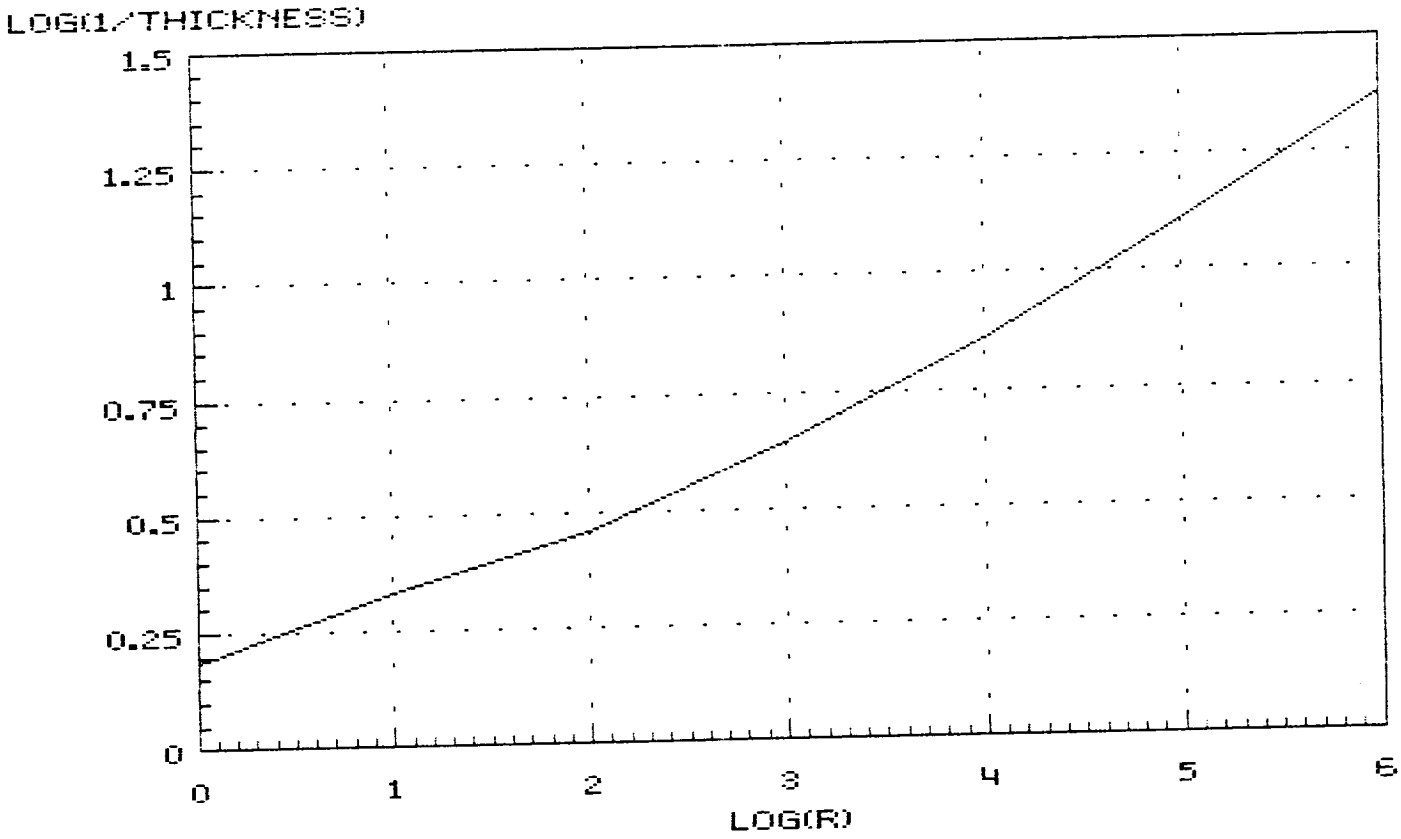

Figure 5. Logarithmic Plot of the Thickness Minimum as a Function of the Rayleigh Number, for the Fixed Deficiency Case.

3.2 Plots of Typical Results

Figures 6 through 9 are plots of the concentration distribution solutions c for R values of 1, 100, 10,000 and 1,000,000. The decrease in the thickness of the boundary layer and plume is immediately apparent. For small R, the distortion from the exact no-flow solution c = 1/r is slight. For large R, the flow is so rapid that the concentration deficiency can only diffuse a very small distance into the fluid.

Figures 10 through 13 show the corresponding flow solutions. The stream function is the volume flux per azimuthal radian, flowing between the indicated point and the axis. The flow follows the stream lines. The rapid increase in the values and in the contour increments should be noted.

Figures 14 through 17 show the theta component of the velocity, for the same cases. The contrast is significant. Resolution problems are apparent at the largest Rayleigh number.

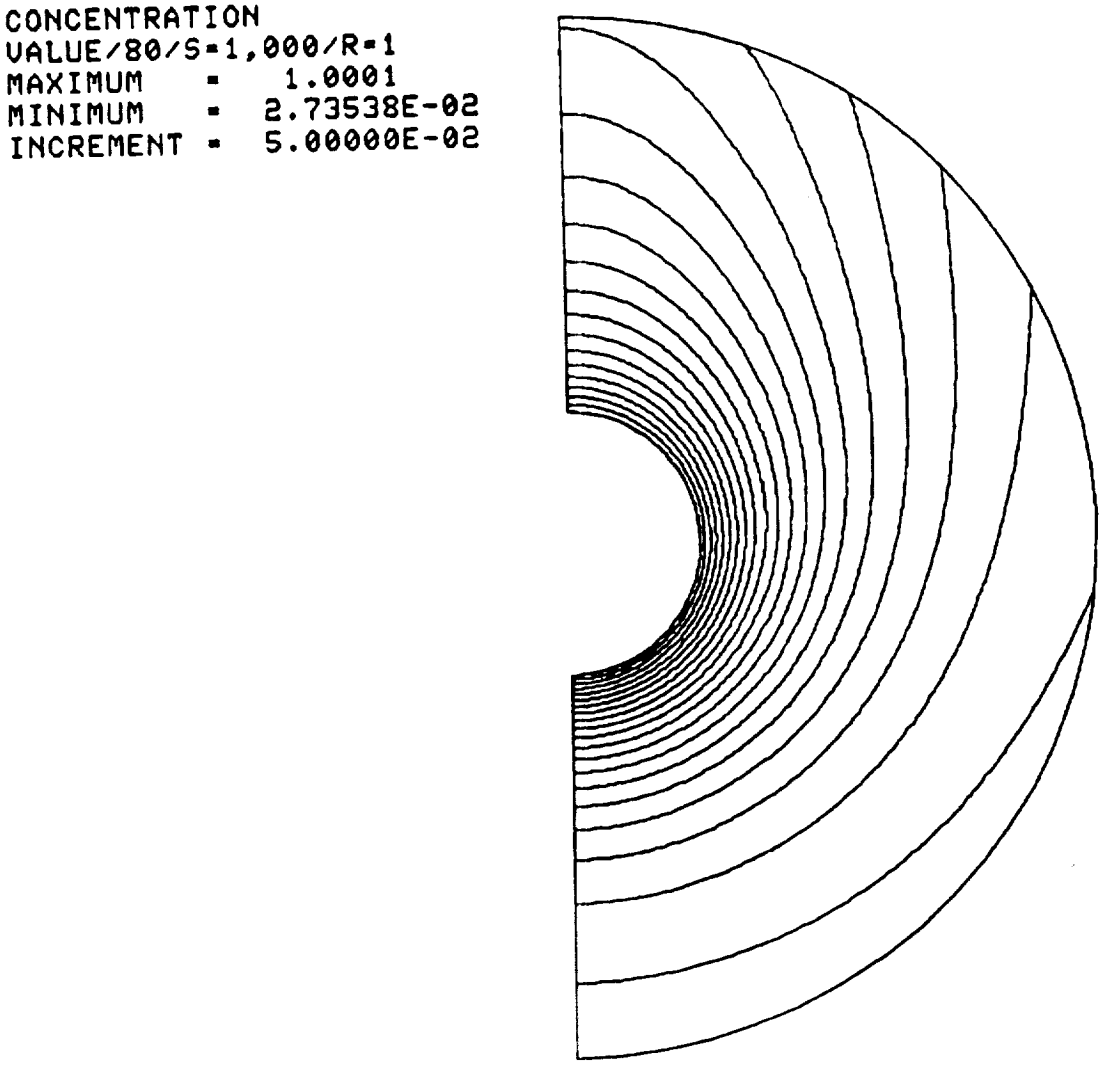

Figure 6. Concentration for Fixed Deficiency Case with S = 1,000 and R = 1

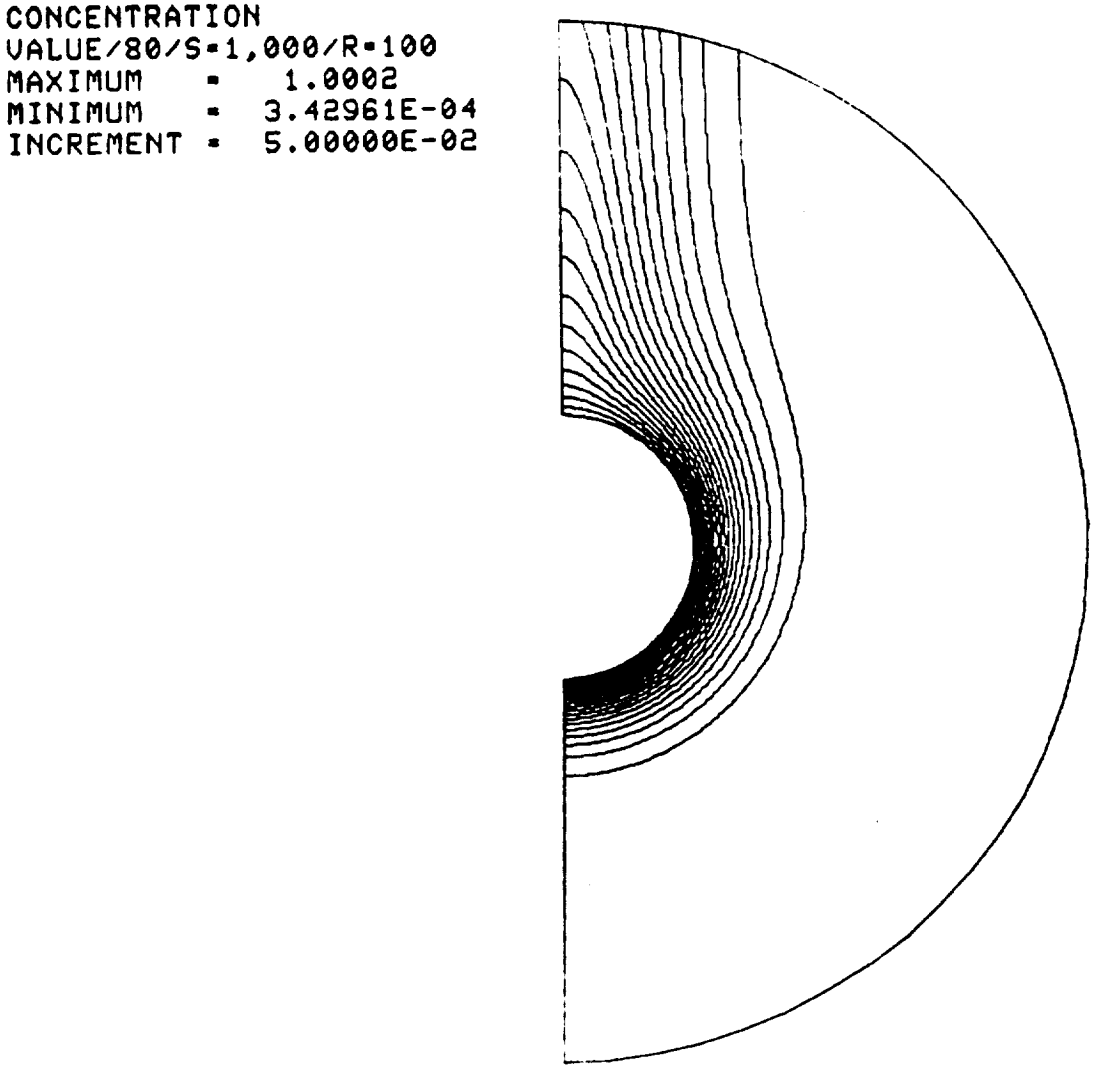

Figure 7. Concentration for Fixed Deficiency Case with S = 1,000 and R = 100

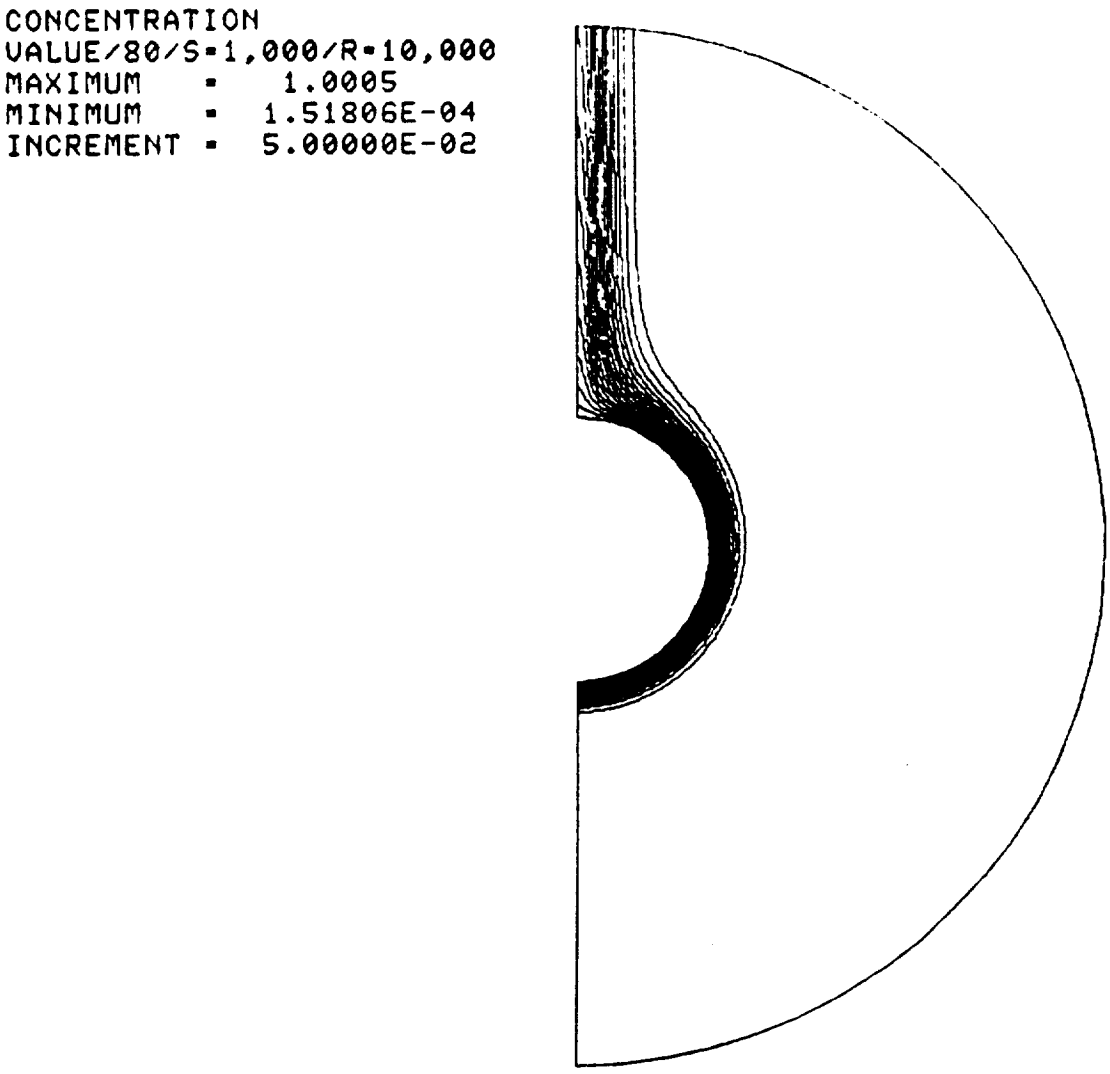

Figure 8. Concentration for Fixed Deficiency Case with S = 1,000 and R = 10,000

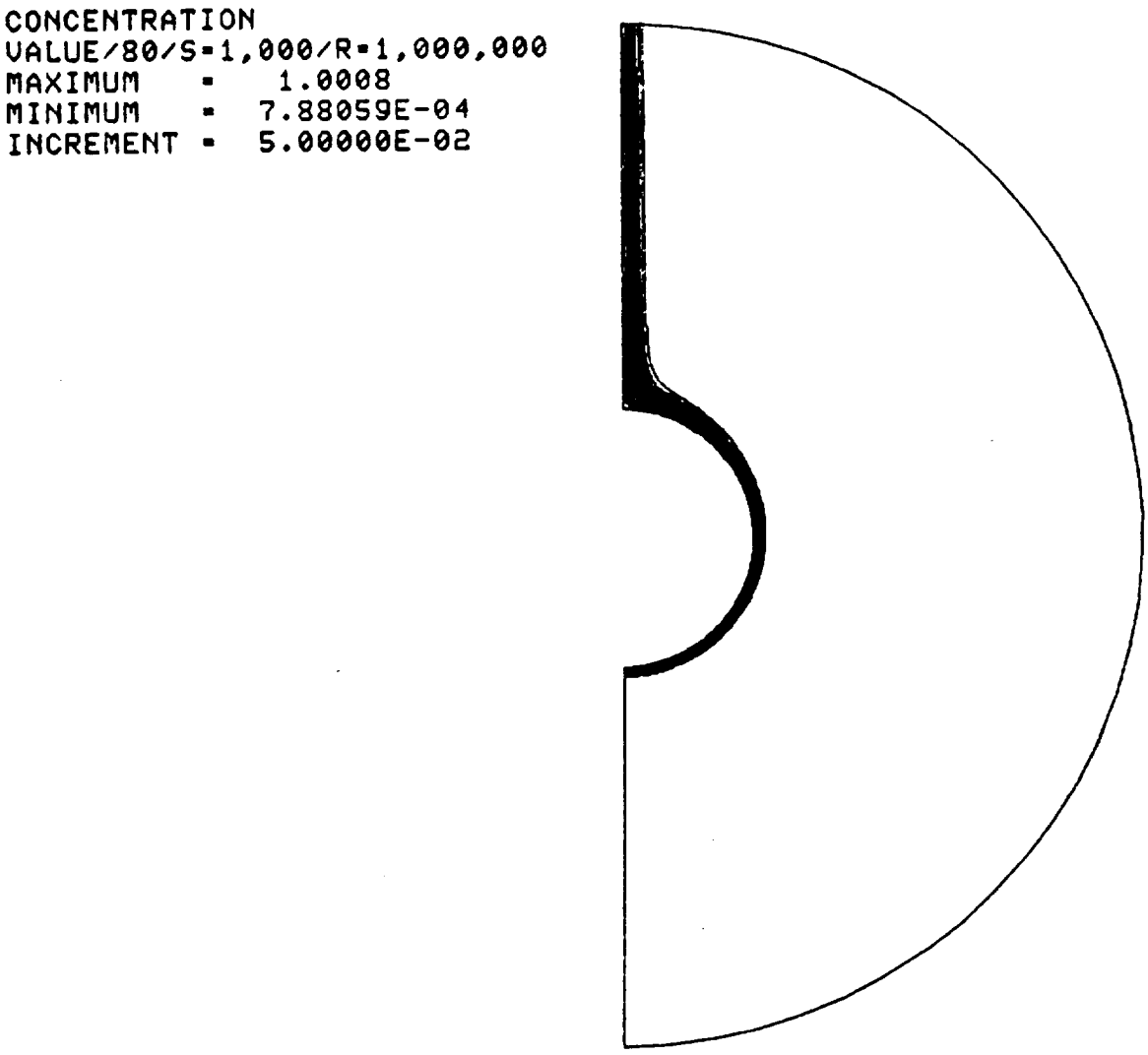

Figure 9. Concentration for Fixed Deficiency Case with S = 1,000 and R = 1,000,000

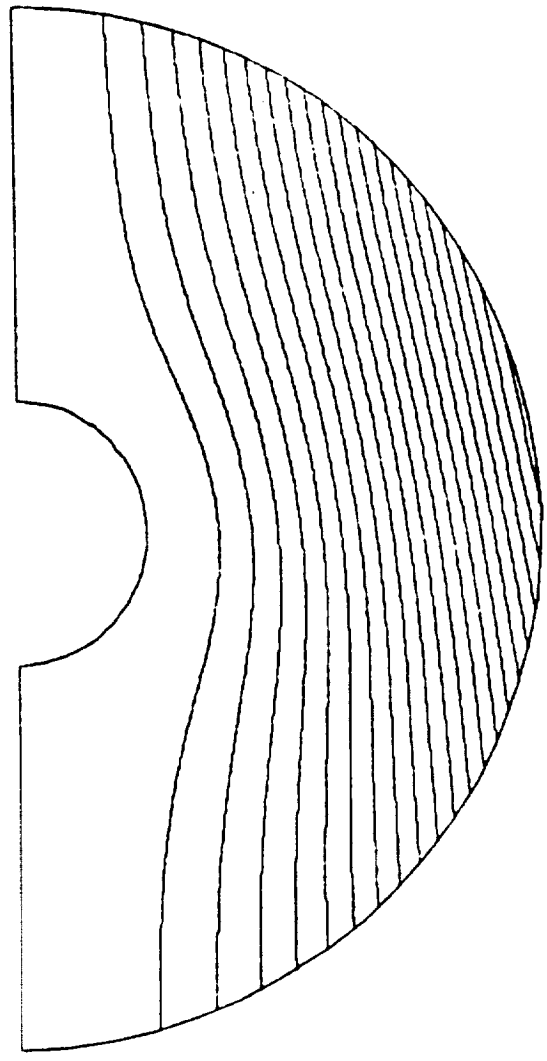

STREAM FUNCTION
VALUE/80/S=1,000/R=1
MAXIMUM = 1.25743E-07
MINIMUM = -8.2172
INCREMENT = 0.40000

Figure 10. Stream Function for Fixed Deficiency Case with S = 1,000 and R = 1

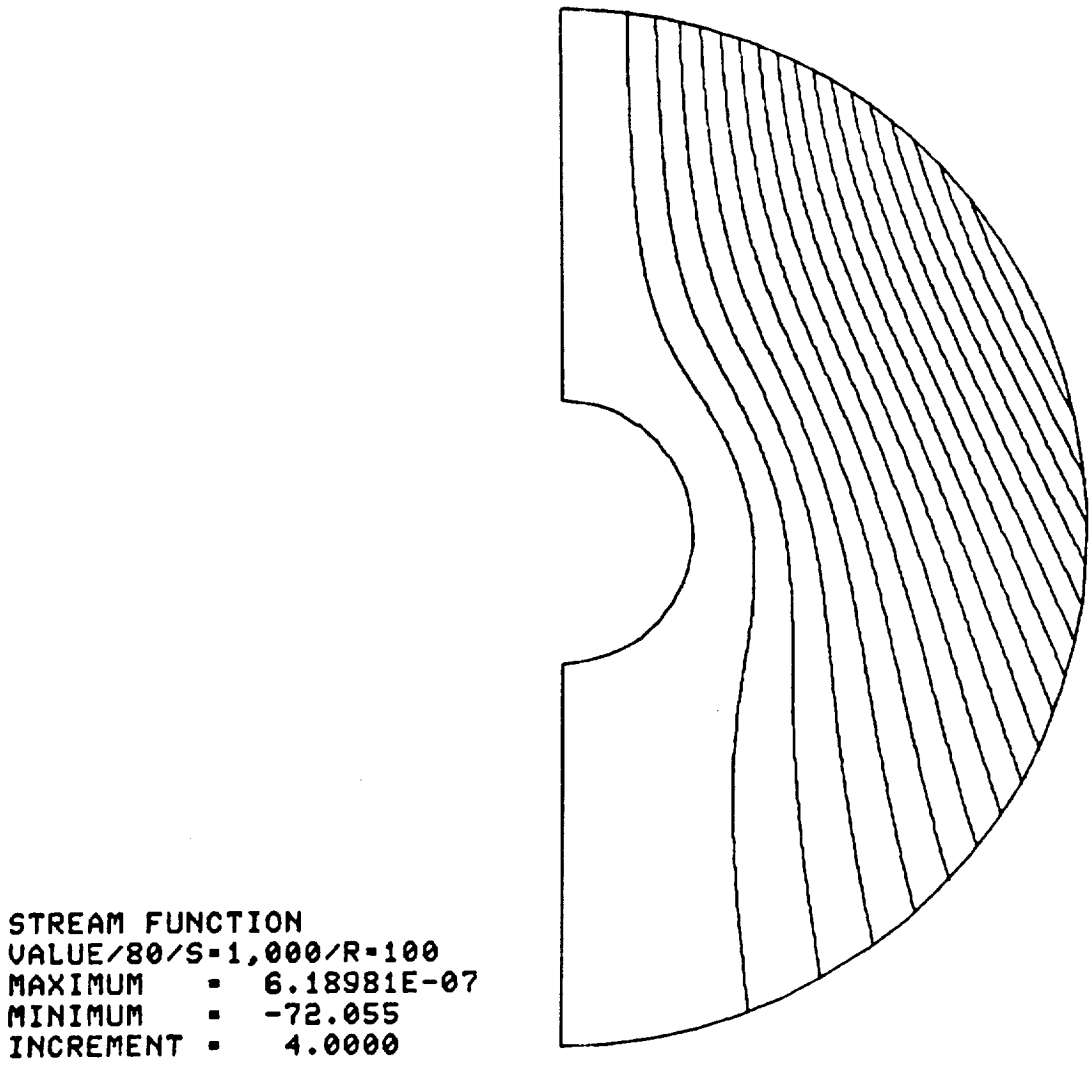

Figure 11. Stream Function for Fixed Deficiency Case with S = 1,000 and R = 100

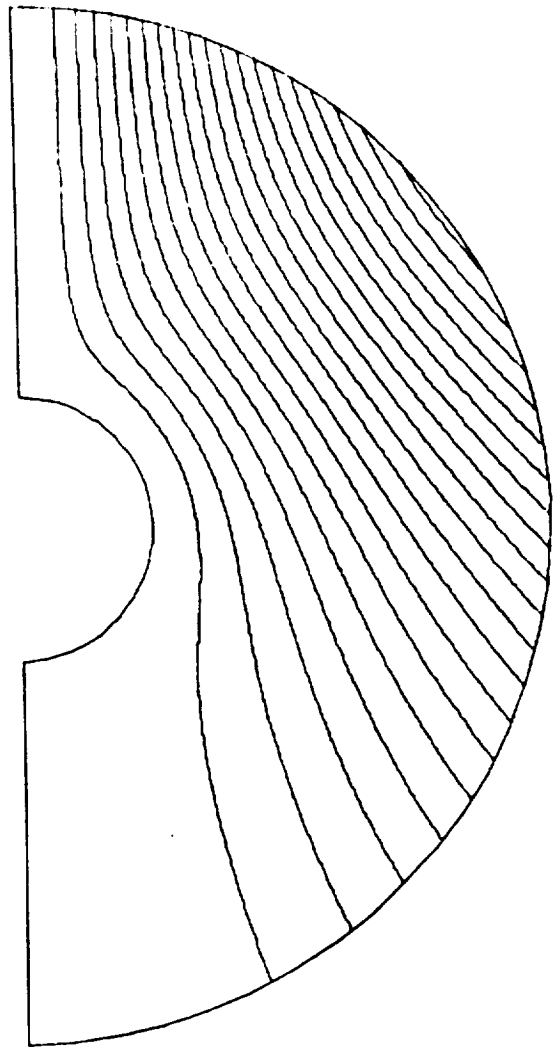

Figure 12. Stream Function for Fixed Deficiency Case with S = 1,000 and R = 10,000

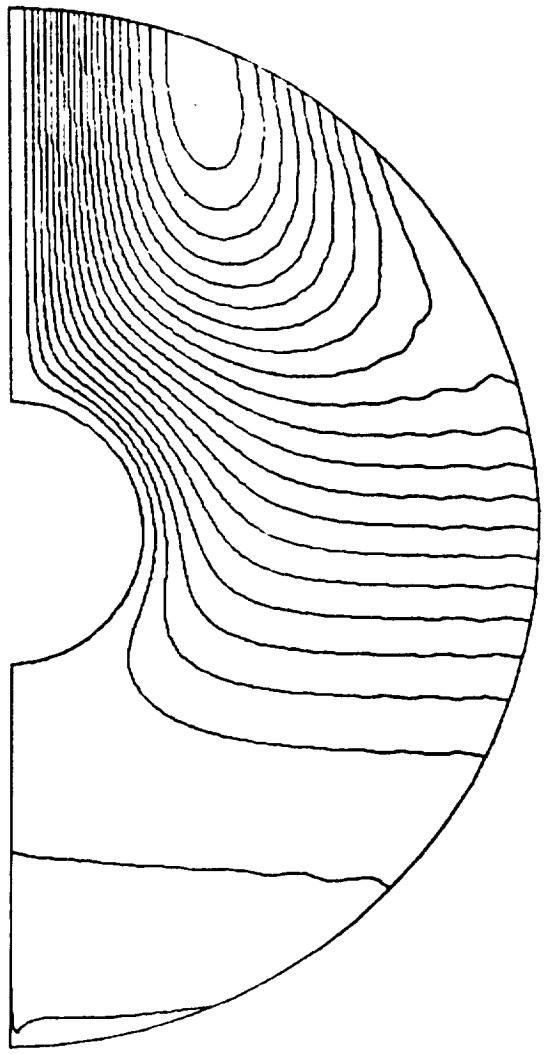

STREAM FUNCTION
VALUE/80/S=1,000/R=1,000,000
MAXIMUM = 2.5662
MINIMUM = -1253.7
INCREMENT = 60.000

Figure 13. Stream Function for Fixed Deficiency Case with S = 1,000 and R = 1,000,000

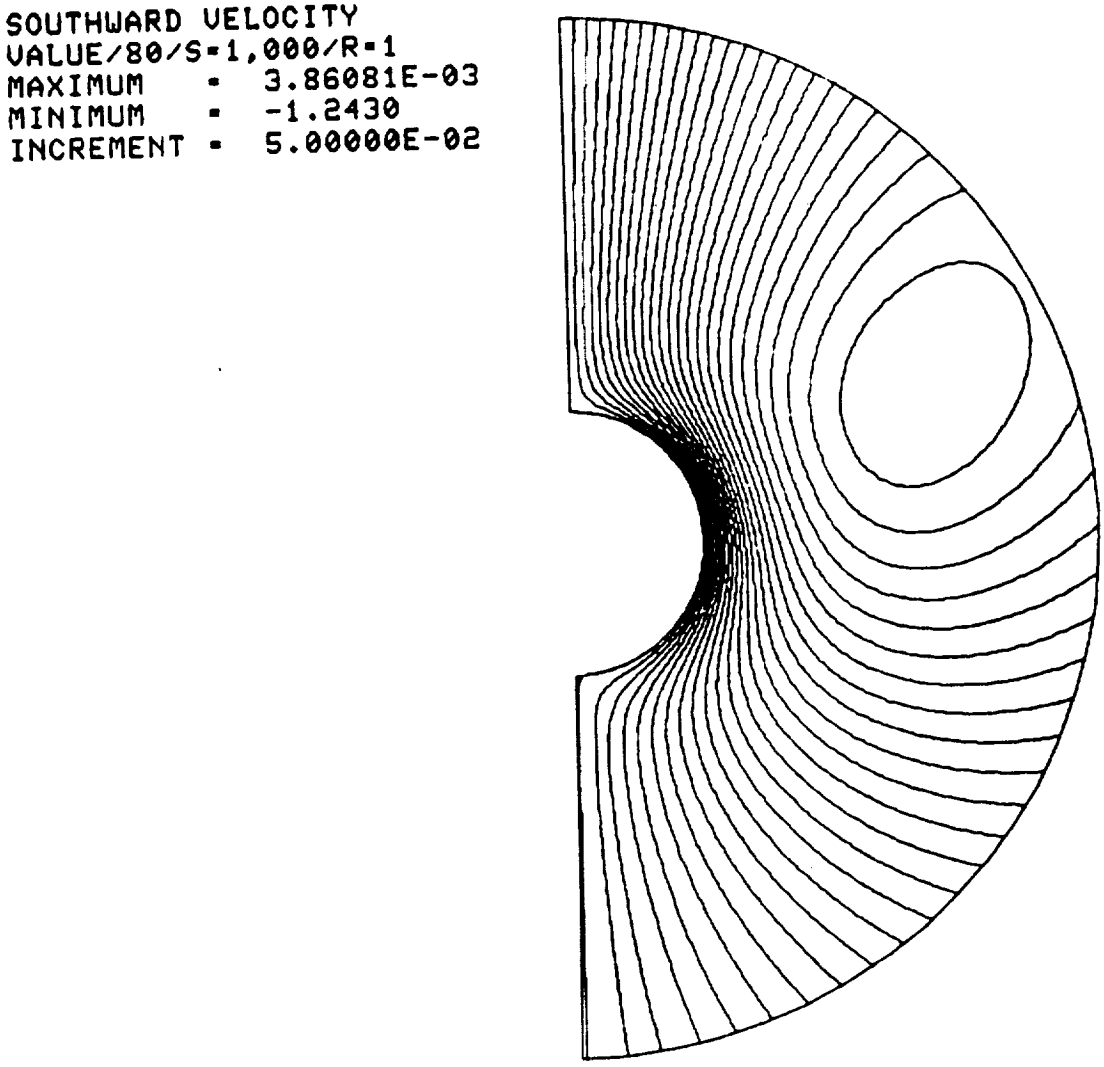

Figure 14. Theta Velocity Component for Fixed Deficiency Case with S = 1,000 and R = 1

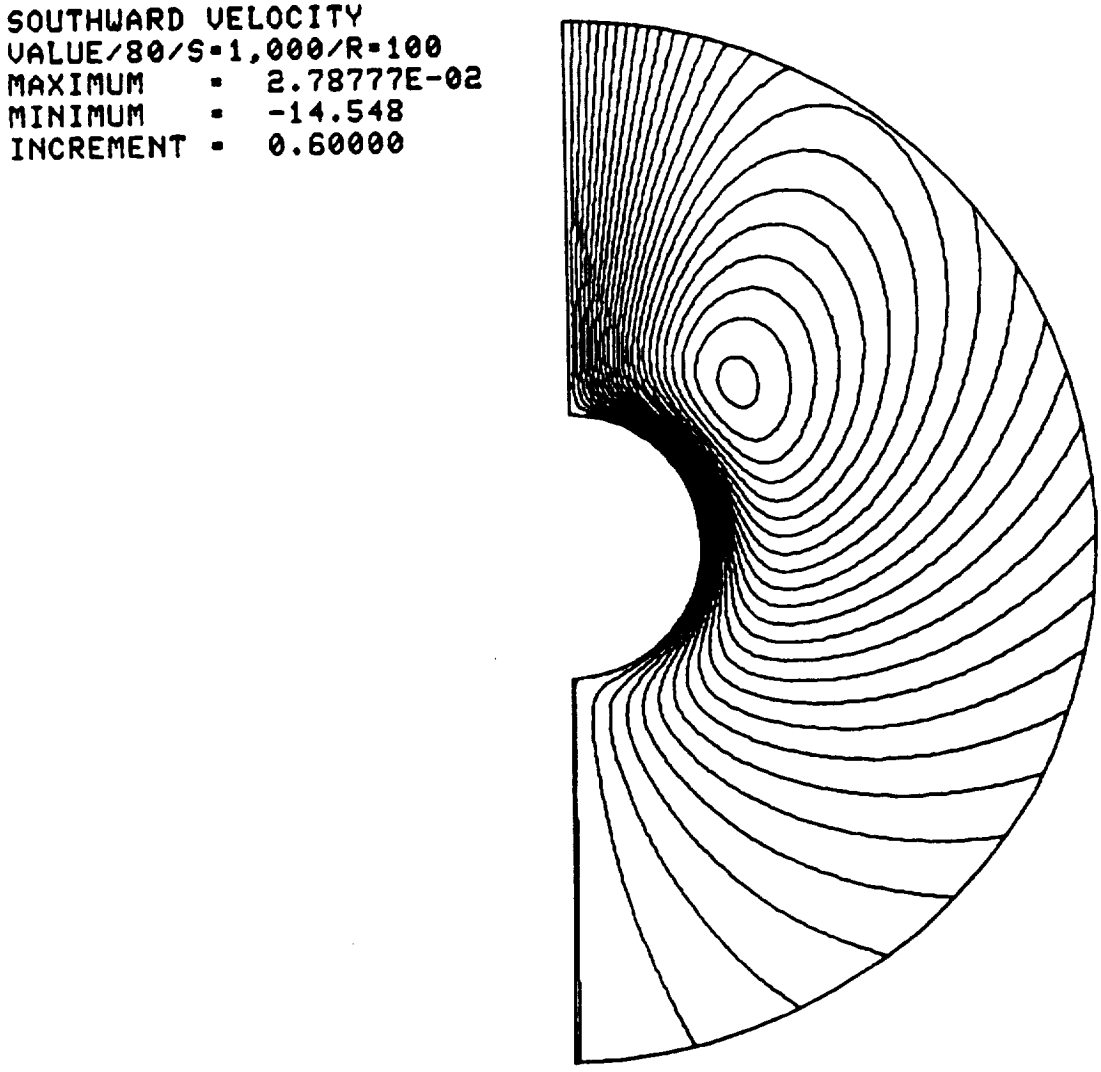

Figure 15. Theta Velocity Component for Fixed Deficiency Case with S = 1,000 and R = 100

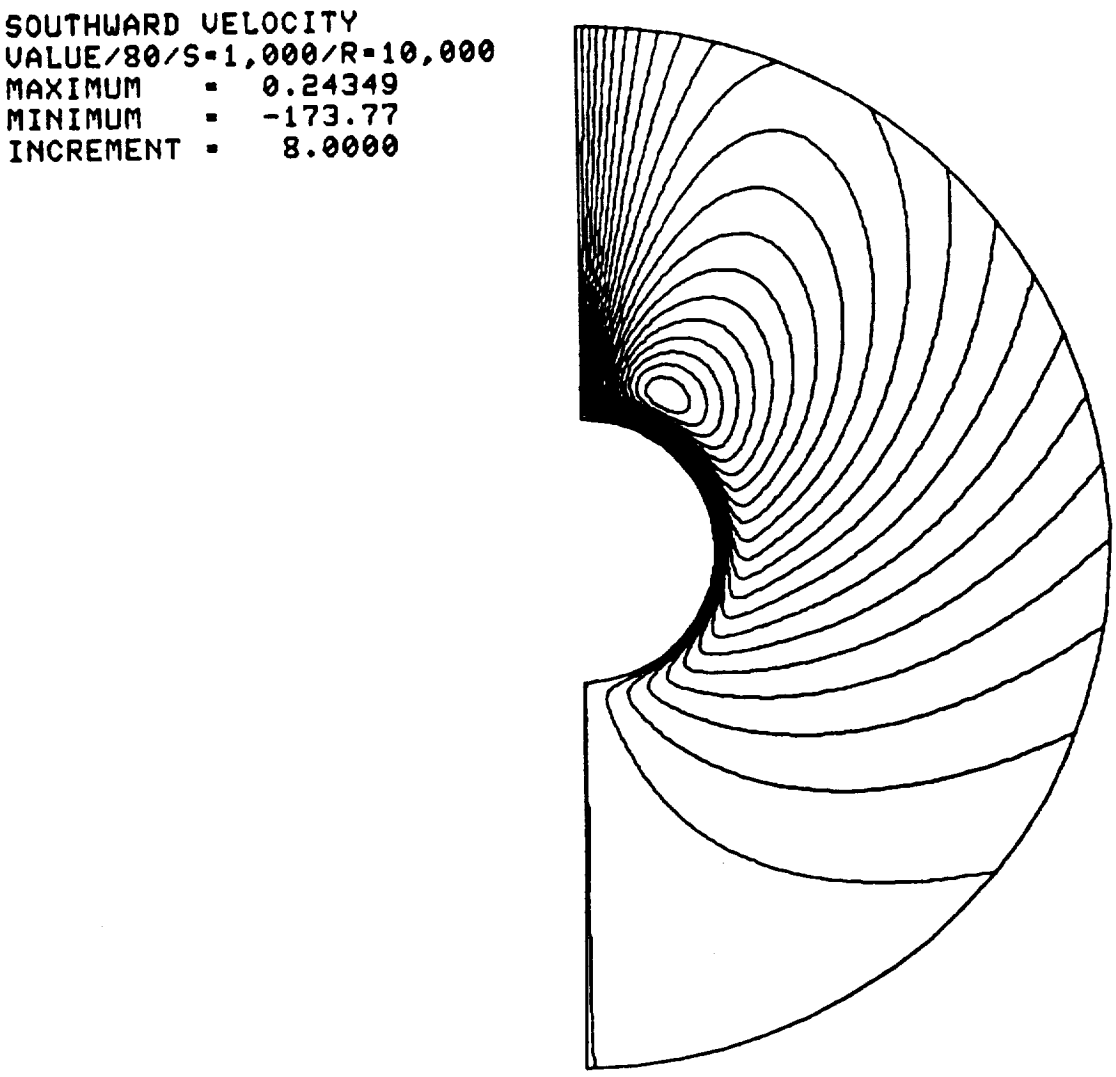

Figure 16. Theta Velocity Component for Fixed Deficiency Case with S = 1,000 and R = 10,000

SOUTHWARD VELOCITY
VALUE/80/S=1,000/R=1,000,000
MAXIMUM = 215.47
MINIMUM = -2039.6
INCREMENT = 100.00

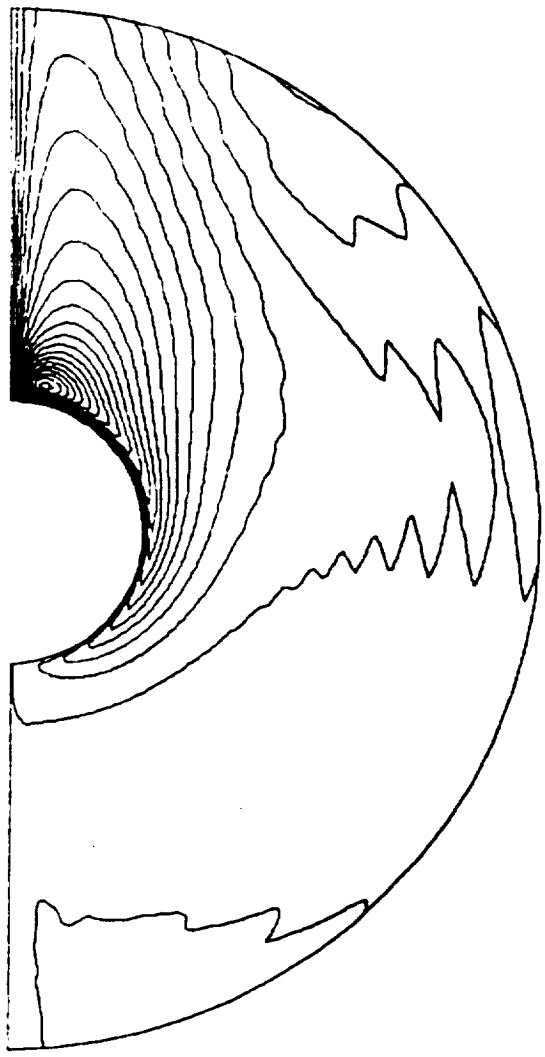

Figure 17. Theta Velocity Component for Fixed Deficiency Case with S = 1,000 and R = 1,000,000

Section 4
FIXED GROWTH RATE

4.1 Summary of Cases

Table 3 is a summary of the fixed growth rate cases which we have computed. For S equal to 1,000, we did R values increasing by factors of ten from one to a million. In addition, we did R values of 1, 1,000, and 100,000, with S equal to 100,000. In each case, the table shows two sets of results, obtained using a 40x40 mesh and using an 80x80 mesh (labeled LOW and HIGH RESOLUTION respectively, to indicate the resolution). For each case and resolution, three numerical values are shown:

the maximum shear magnitude; and

the maximum and minimum concentration.

		LOW RESOLUTION			HIGH RESOLUTION		
S	R	SHEAR	c_{max}	c_{min}	SHEAR	c_{max}	c_{min}
1,000	1	2.59	0.890	0.710	2.85	0.874	0.690
	10	10.50	0.772	0.542	13.93	0.743	0.508
	100	40.06	0.640	0.409	41.61	0.635	0.403
	1,000	152.29	0.500	0.292	158.29	0.496	0.288
	10,000	572.76	0.372	0.199	601.03	0.368	0.197
	100,000	2121.70	0.266	0.132	2265.10	0.263	0.132
	1,000,000	7658.60			8534.50	0.182	0.086
100,000	1	0.26	0.890	0.710		0.874	0.689
	1,000	152.89	0.500	0.291	169.42	0.496	0.288
	100,000	2125.10	0.274	0.136	2436.80	0.262	0.132

Table 3. Summary of Numerical Results for the Fixed Growth Rate Cases

The following points should be noted about these results.

First, the error of the high-resolution case is less than a quarter of the error of the low resolution case, because the method parameters and the domain choice RB were improved in each case for the high-resolution run, based on the low-resolution results. Comparing the numbers, it can be seen that all the high resolution results have satisfactory accuracy.

Secondly, the differences between the results for the two different values of S are very small. For this reason, we did not do an exhaustive analysis of the effect of S. This result is consistent with the analysis in Section 1; since S enters the equations only in the momentum term, which is multiplied by the reciprocal of S.

Thirdly, the maximum of the concentration occurs at the end of the plume, and is of relatively little significance. The minimum of the concentration is a measure of the reciprocal of the boundary layer thickness, since the normal derivative is -1.

Fourthly, the boundary layer thickness becomes very small as R increase, as predicted theoretically in Section 1.8. For this reason, the input data

used decreasing values of the parameters DRB and DTHL (cf. Section 2.2) as R increased, in order to resolve the boundary layer and plume.

Figure 18 is a logarithmic plot of the maximum shear on the interface, as a function of the Rayleigh number R. The slope at large R is close to the predicted value of 3/5. We did not go to small enough R to obtain the predicted slope of unity in that region.

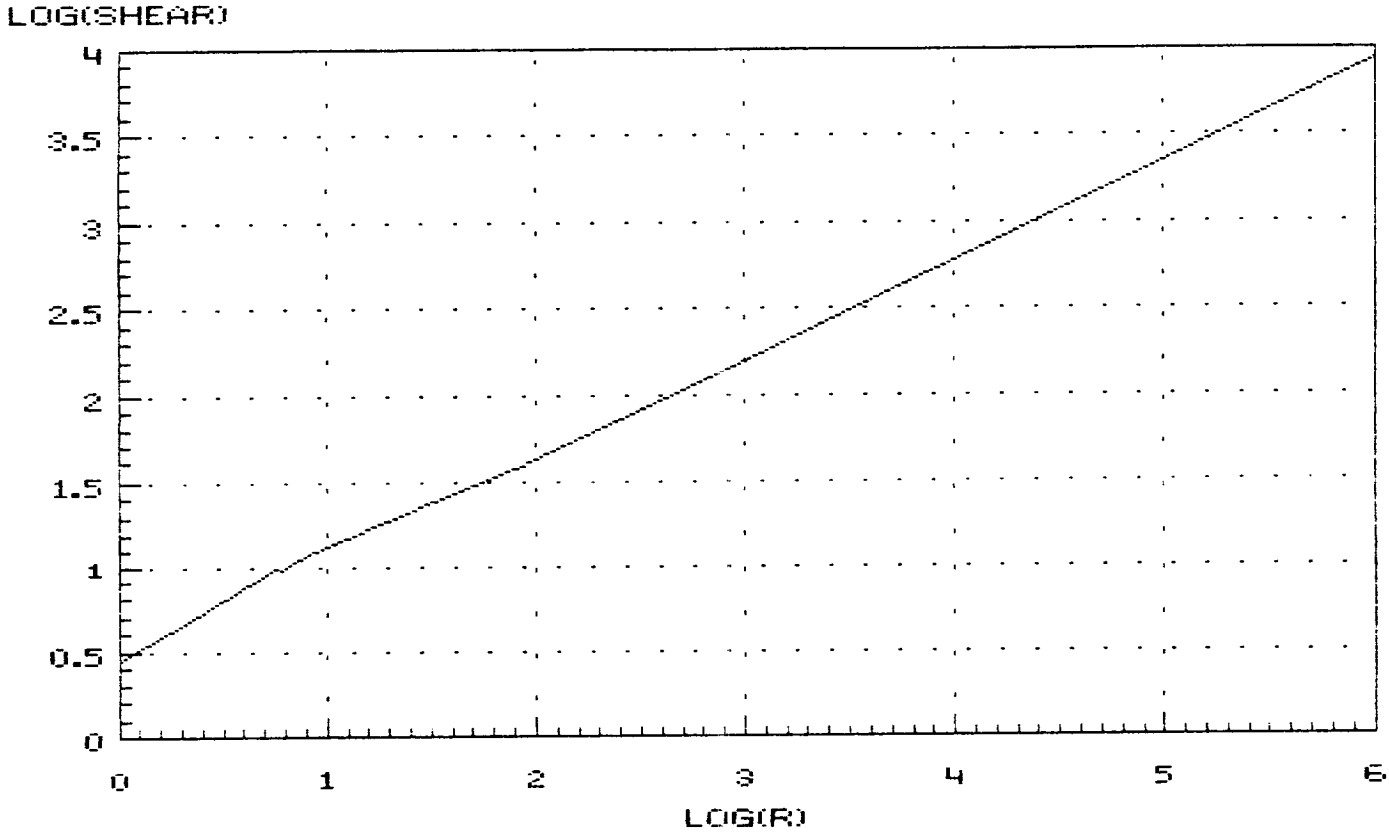

Figure 18. Logarithmic Plot of the Shear Maximum as a Function of the Rayleigh Number, for the Fixed Growth Rate Case.

Figure 19 is a logarithmic plot of the boundary layer thickness as a function of R. Again, the slope is close to the predicted value of 1/5, for large R. For small R, the analytic solution T = 1/r is approached, with constant thickness unity.

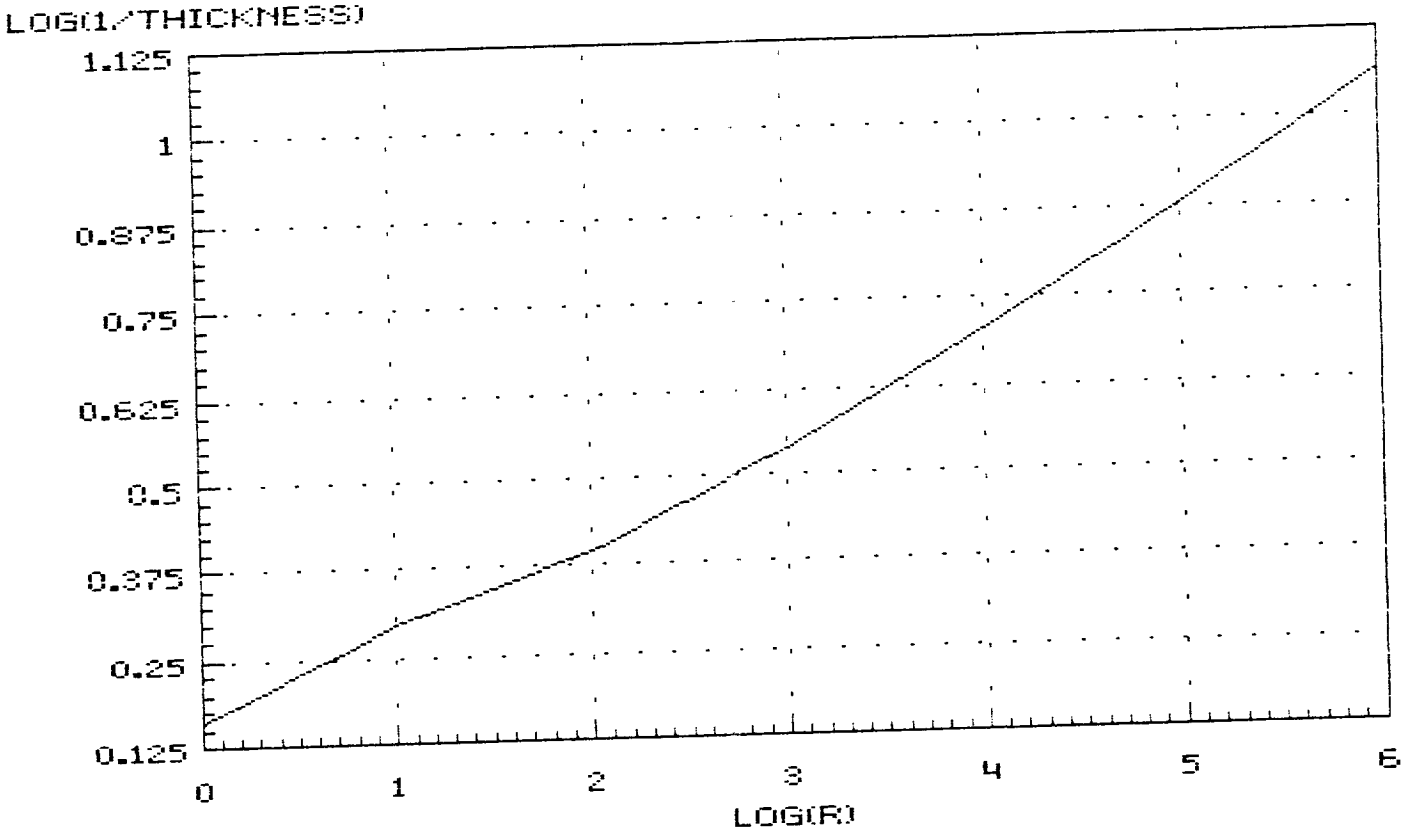

Figure 19. Logarithmic Plot of the Thickness Minimum as a Function of the Rayleigh Number, for the Fixed Growth Rate Case.

4.2 Plots of Typical Results

Figures 20 through 23 are plots of the concentration distribution solutions c for R values of 1, 100, 10,000 and 1,000,000. The decrease in the thickness of the boundary layer and plume is immediately apparent. For small R, the distortion from the exact no-flow solution c = 1/r is slight. For large R, the flow is so rapid that the concentration deficiency can only diffuse a very small distance into the fluid.

Figures 24 through 27 show the corresponding flow solutions. The stream function is the volume flux per azimuthal radian, flowing between the indicated point and the axis. The flow follows the stream lines. The rapid increase in the values and in the contour increments should be noted.

Figures 28 through 31 show the theta component of the velocity, for the same cases. The contrast is significant. Resolution problems are apparent at the largest Rayleigh number.

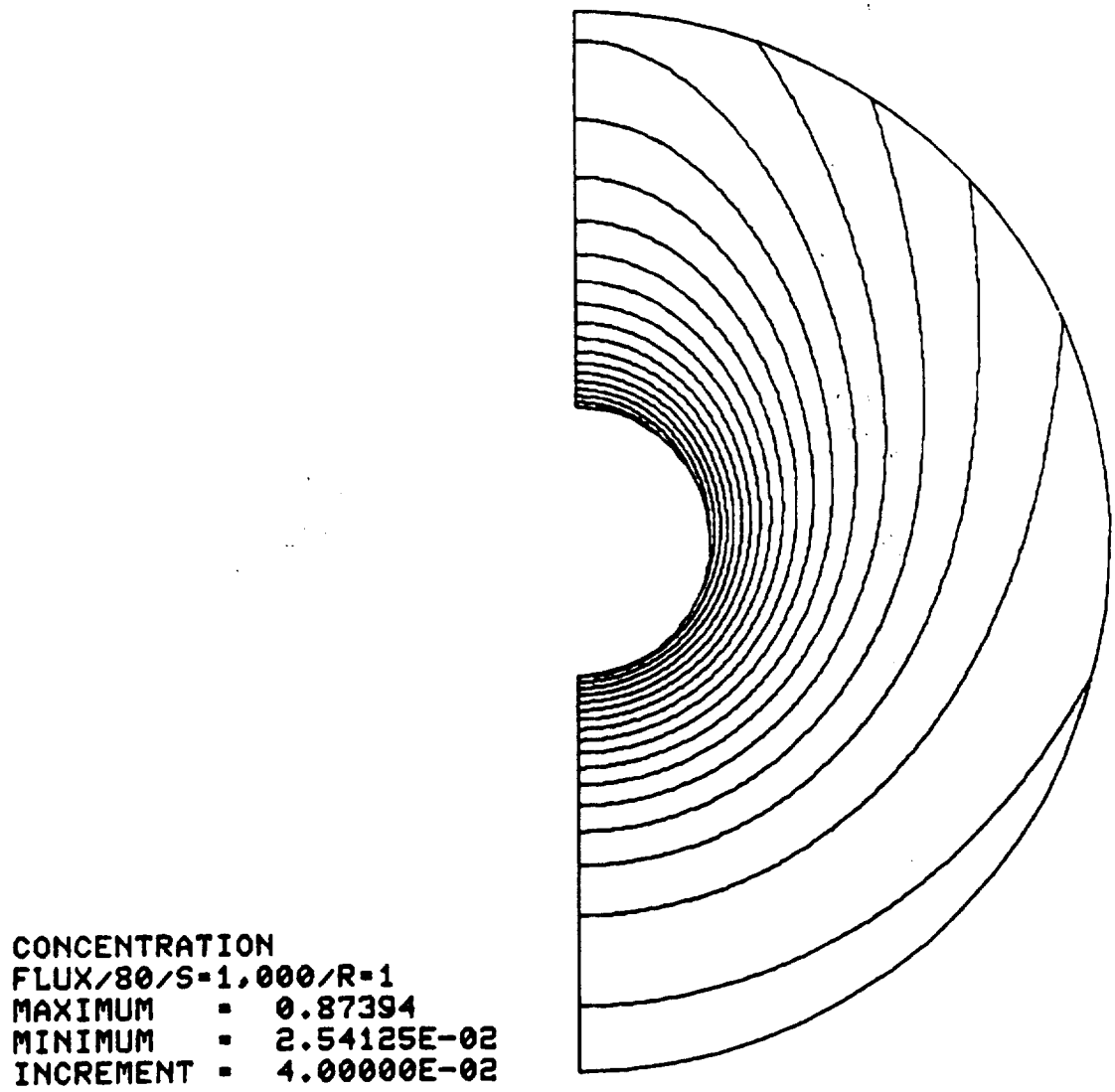

Figure 20. Concentration for Fixed Growth Rate Case with S = 1,000 and R = 1

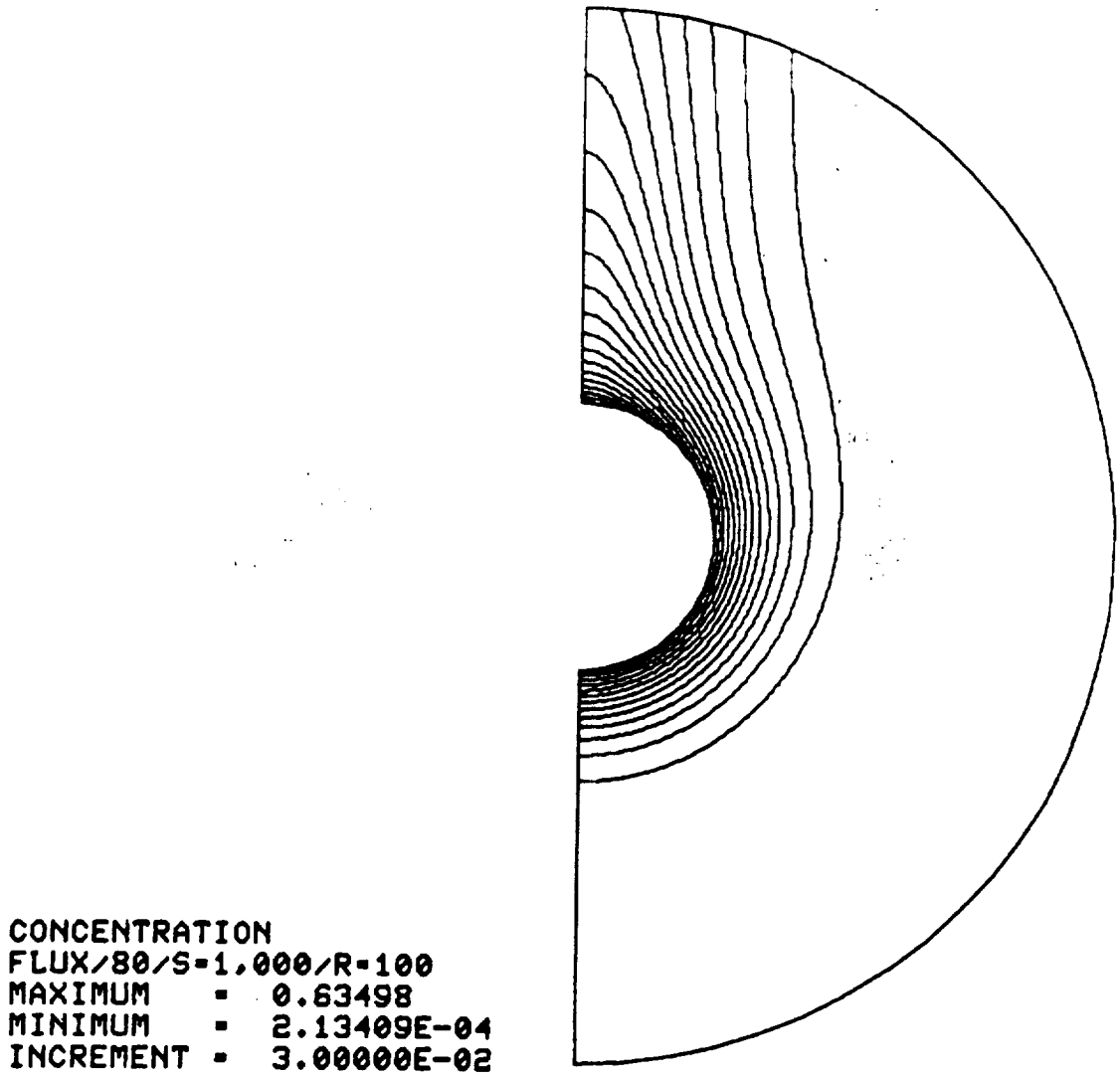

Figure 21. Concentration for Fixed Growth Rate Case with S = 1,000 and R = 100

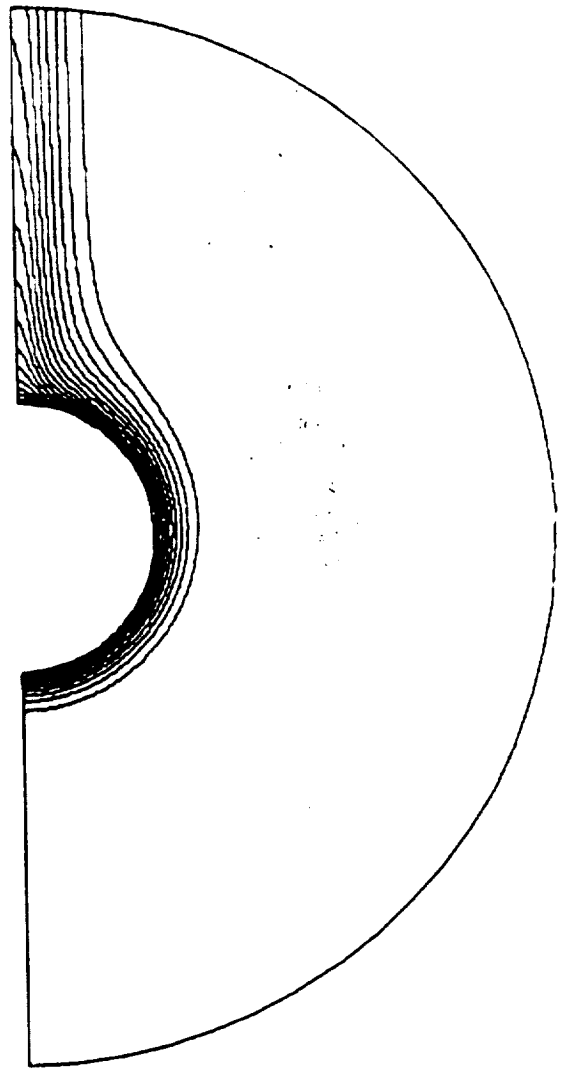

Figure 22. Concentration for Fixed Growth Rate Case with S = 1,000 and R = 10,000

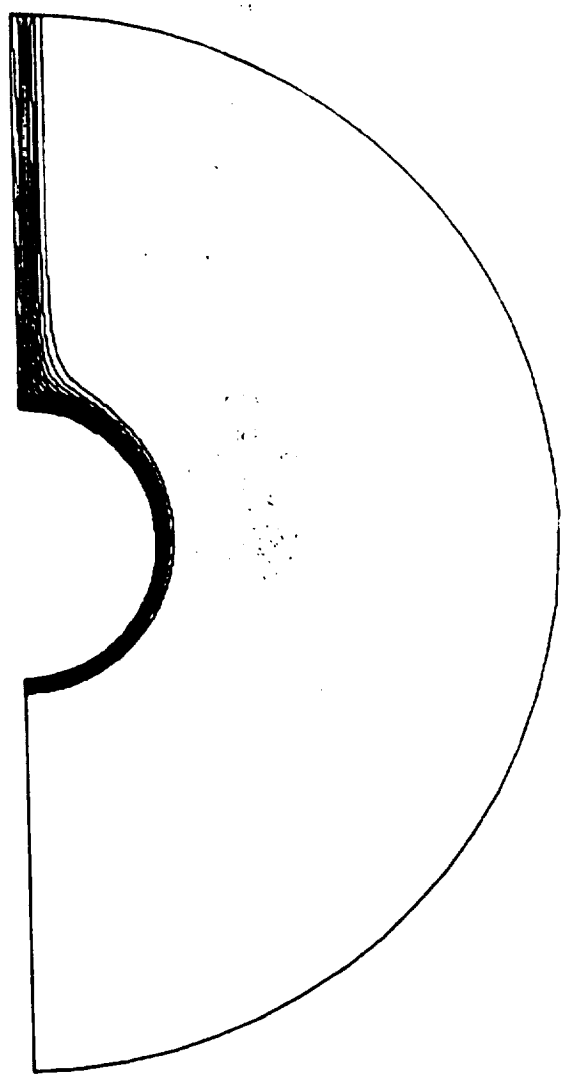

Figure 23. Concentration for Fixed Growth Rate Case with S = 1,000 and R = 1,000,000

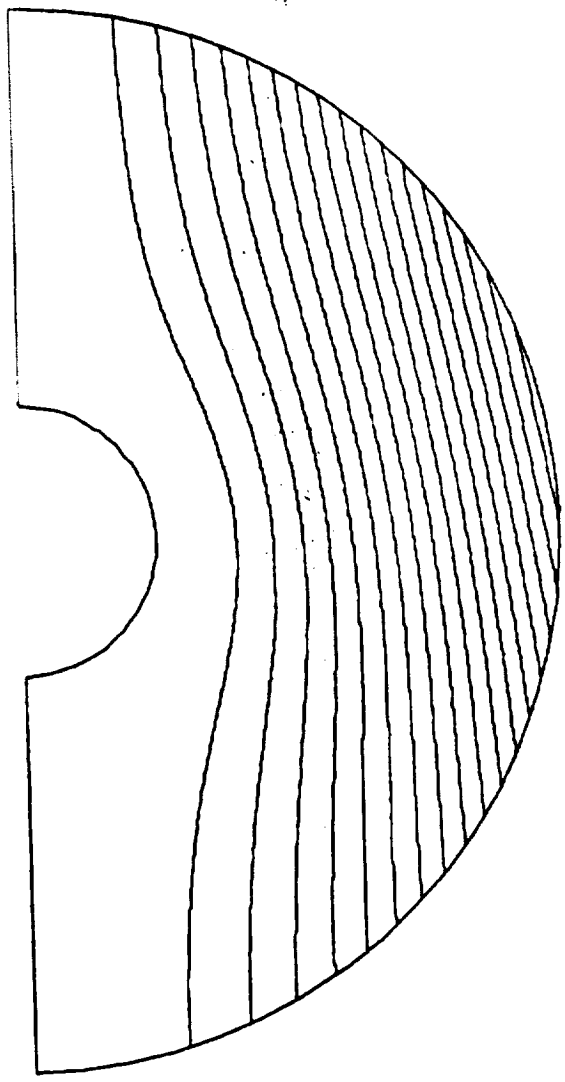

Figure 24. Stream Function for Fixed Growth Rate Case with S = 1,000 and R = 1

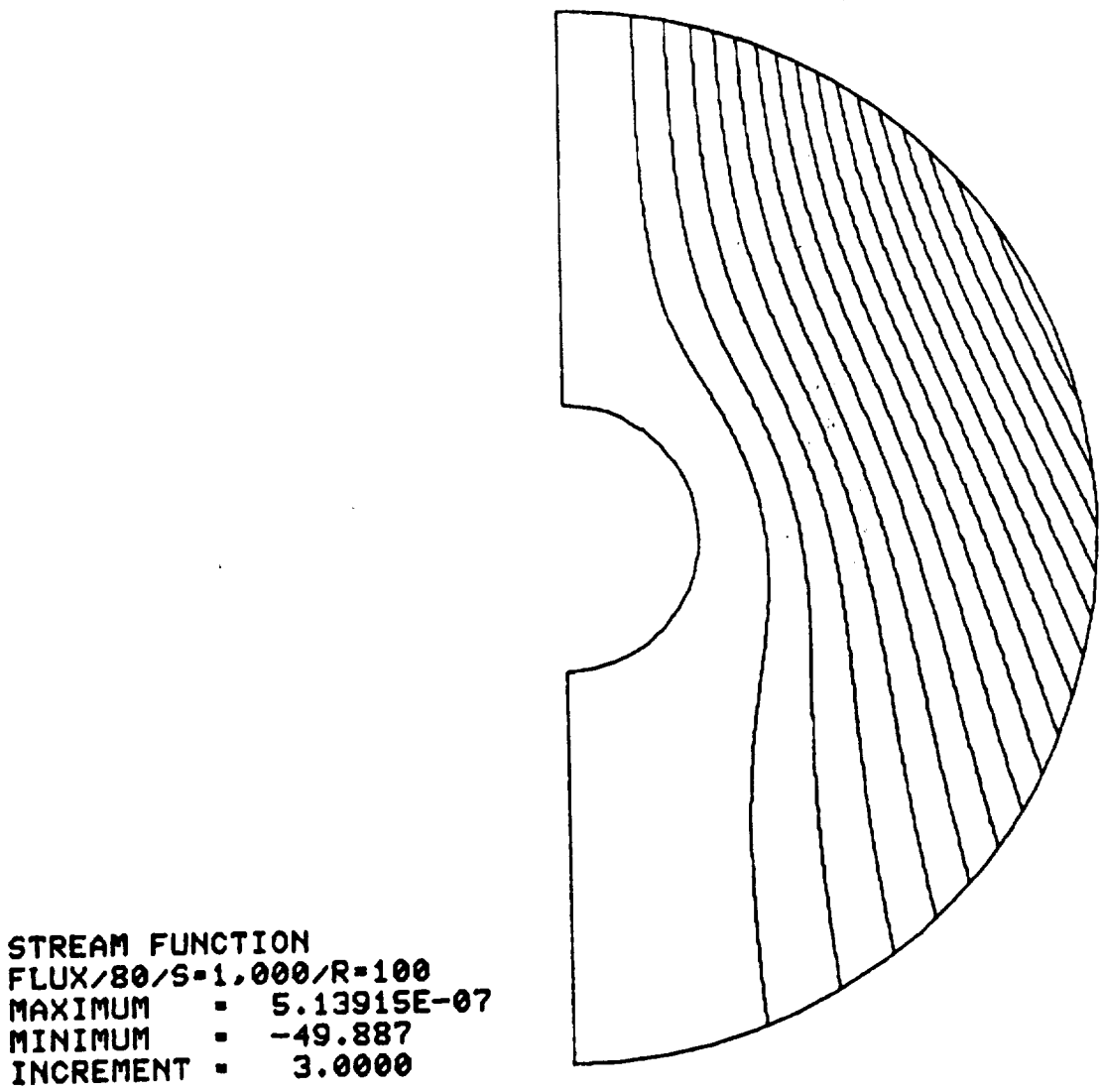

Figure 25. Stream Function for Fixed Growth Rate Case with S = 1,000 and R = 100

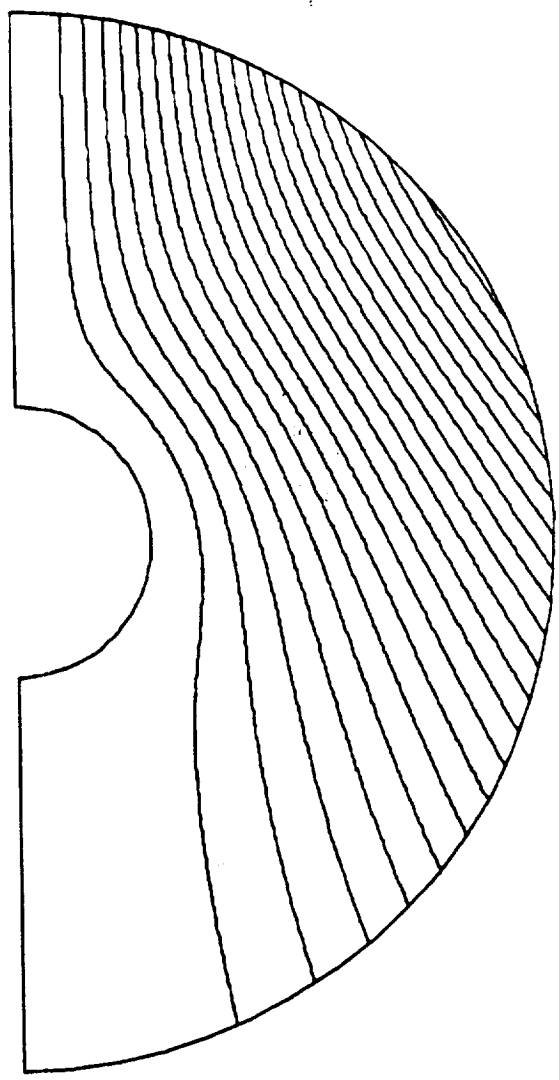

Figure 26. Stream Function for Fixed Growth Rate Case with S = 1,000 and R = 10,000

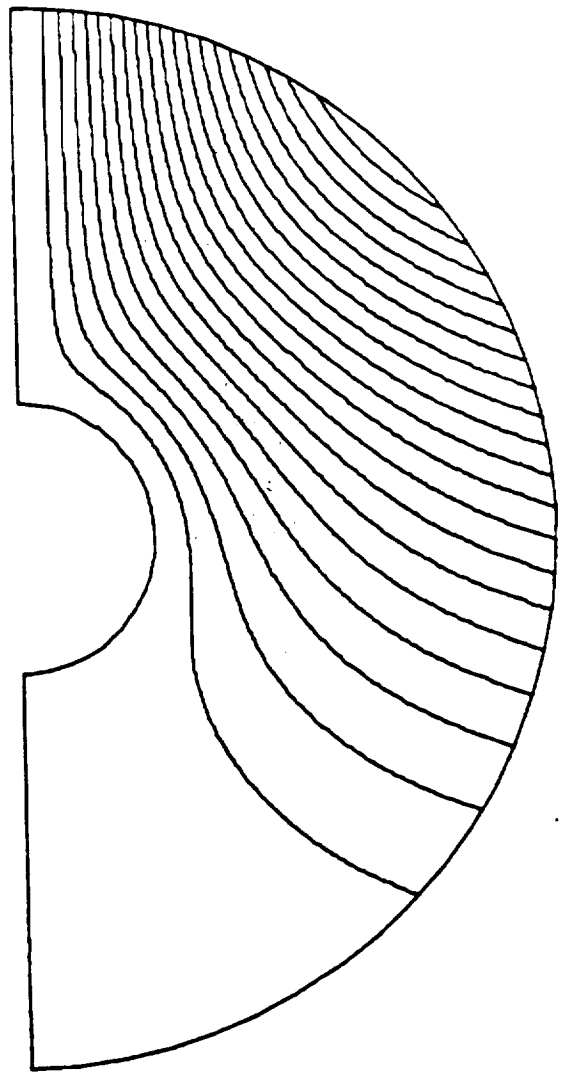

Figure 27. Stream Function for Fixed Growth Rate Case with S = 1,000 and R = 1,000,000

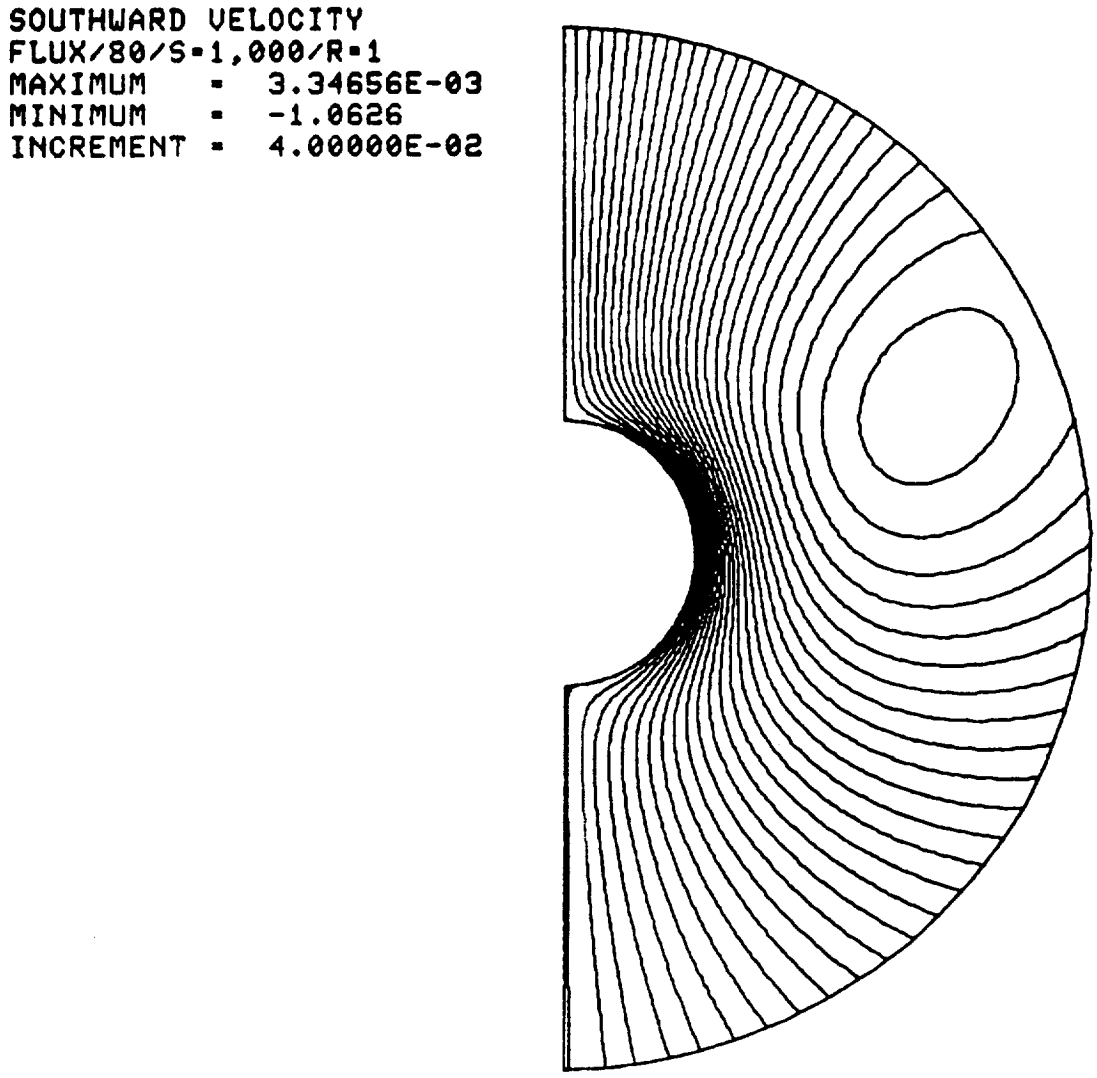

Figure 28. Theta Velocity Component for Fixed Growth Rate Case with S = 1,000 and R = 1

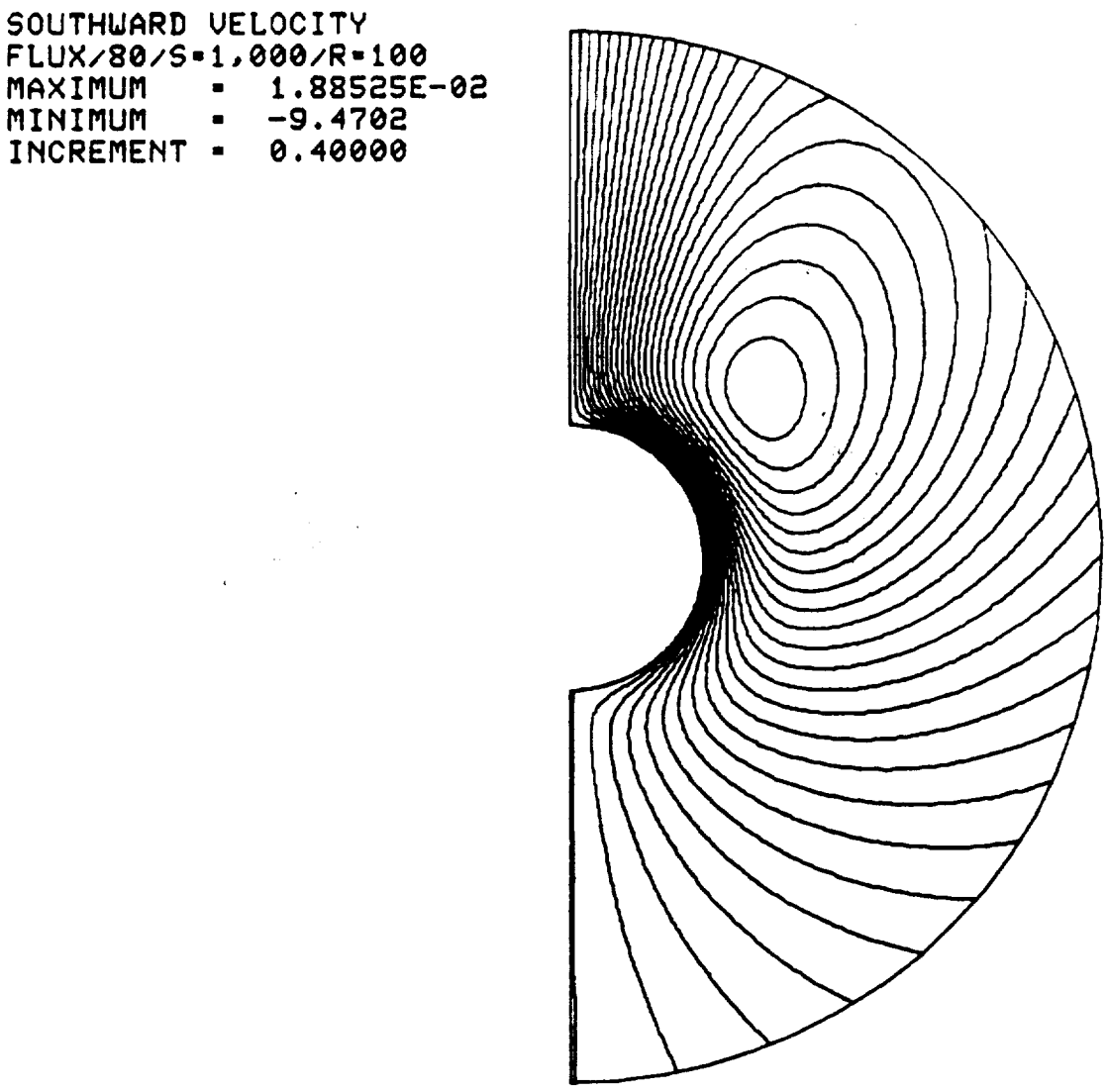

Figure 29. Theta Velocity Component for Fixed Growth Rate Case with S = 1,000 and R = 100

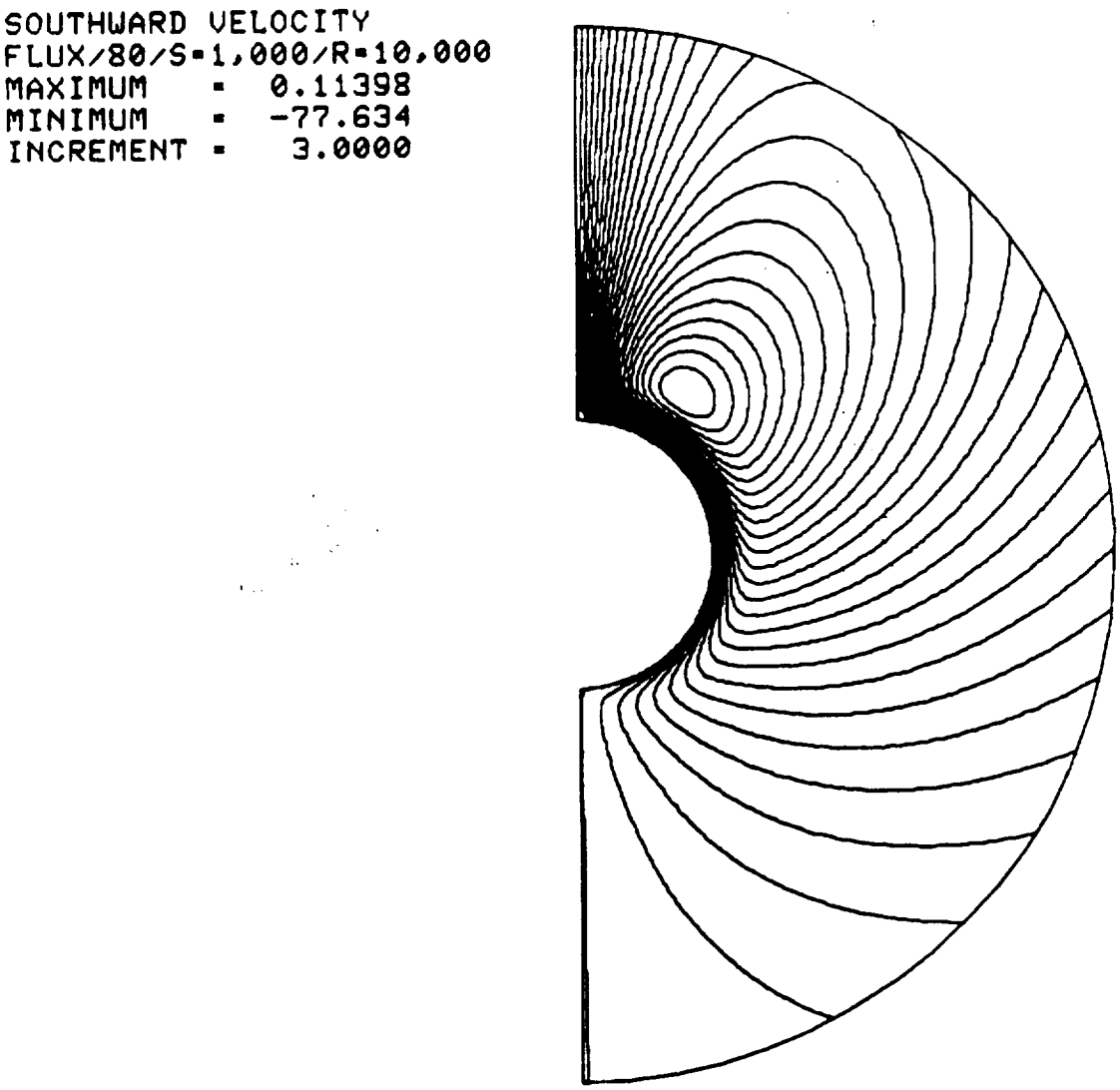

Figure 30. Theta Velocity Component for Fixed Growth Rate Case with S = 1,000 and R = 10,000

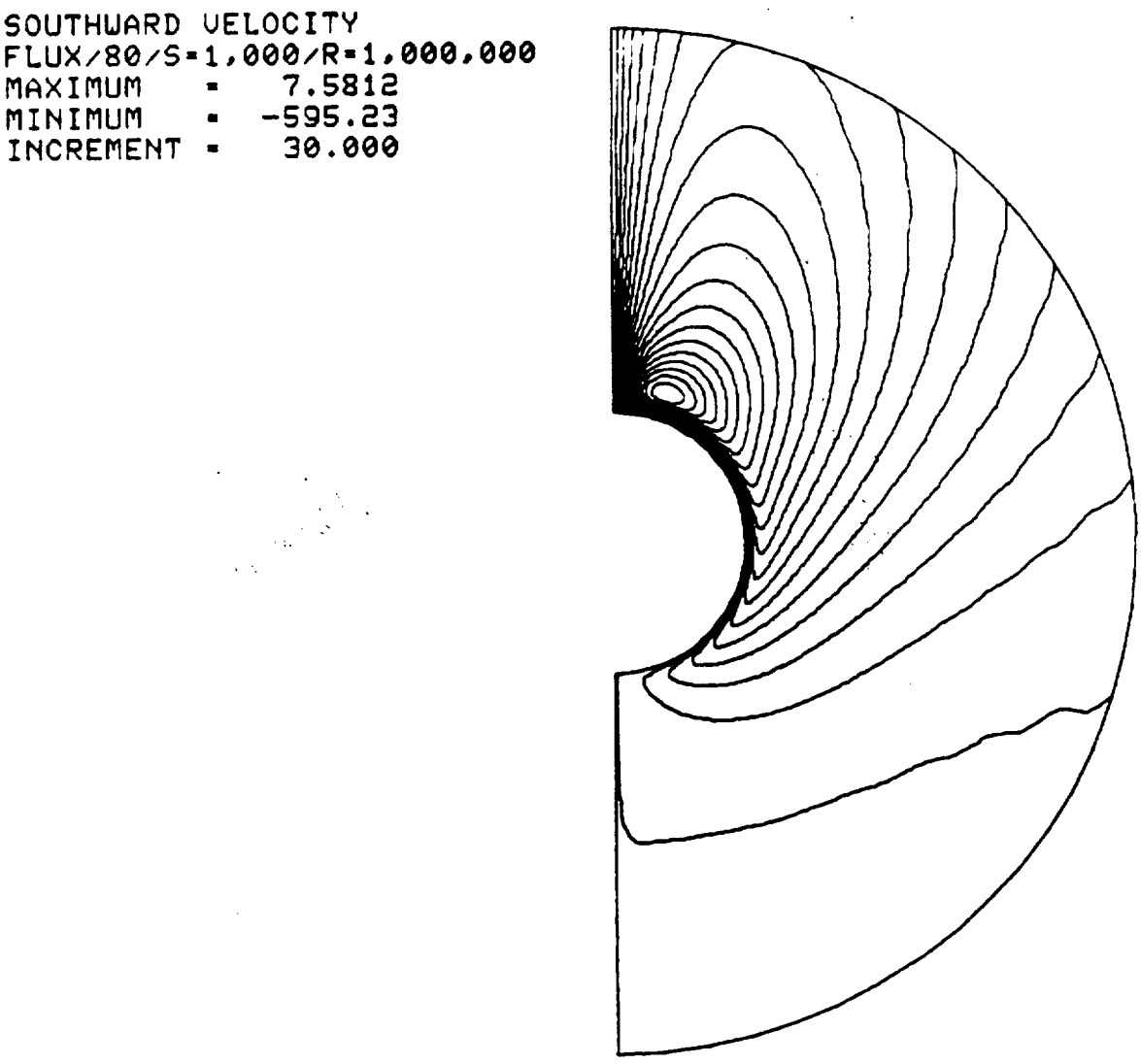

Figure 31. Theta Velocity Component for Fixed Growth Rate Case with S = 1,000 and R = 1,000,000

Section 5
CONCLUSIONS

We have suggested that the main reason for the difficulty in growing protein crystals beyond a certain rather limited size in terrestrial gravity is the accumulation of crystal defects caused by crystal growth in a shear convection flow. This would apply both to a hanging drop configuration and to growth of a supported crystal. The configuration of the added molecules is modified by the shear flow.

We have analyzed the easier case of the growth of a supported protein crystal from a homogeneous supersaturated protein solution. We assumed that the crystal remains spherical, with its growth rate negligible compared with the flow speeds. We assumed that the surrounding supersaturated protein solution is effectively infinite, and homogeneous at infinity, and we neglected sting effects.

We derived the non-dimensional equations. We obtained order of magnitude estimates for the velocity shear on the protein boundary and for the boundary layer thickness, as functions of the dimensionless Rayleigh number, in the two relevant limits of fixed density deficiency at the interface, and of fixed growth rate. We demonstrated that with this non-dimensionalization, the Schmidt number and the momentum term can be dropped from the analysis.

We derived the following table for the dimensional shear in the limits of small and large R, for fixed deficiency and for fixed growth rate.

	Fixed Deficiency	Fixed Growth Rate
$R \ll 1$	$\frac{gCa}{\nu}$	$\frac{gCa^2}{\nu}$
$R \gg 1$	$(gC/R\nu)^{3/4}(Da)^{1/4}$	$(gC'/D\nu)^{3/5}(Da)^{2/5}$

As a crystal grows, R increases rapidly. If the critical value of the shear (where crystal damage occurs) is reached while R is still small compared with unity, then the shear is strongly dependent on radius, and therefore the critical radius is relatively insensitive to the other parameters. On the other hand, once R is greater than one, small changes in the other parameters may allow substantial changes in a.

We solved the equation numerically for Rayleigh numbers in the range from one to a million, and for Schmidt numbers from 1,000 to 100,000. The results confirmed our analysis. We produced plots of the concentration and flow solutions over the whole range. This work as done using an existing computer code, developed under NASA sponsorship for a different application.

REFERENCES

Marc L. Pusey, Robert S. Snyder, and Robert E. Naumann (1986), "Protein Crystal Growth. Growth Kinetics for Tetragonal Lysozyme Crystals". J. Biol. Chem. 261, pp. 6524-6529.

Daniel Carter (1987), private communication.

R. Giordano, A. Salleo, S. Salleo, and F. Wanderlingh (1979), "Viscosity and density of Lysozyme in Water", Physics Letters 70A, pp. 64-66.

G.L. Gilliland and D.R. Davies (1984), Methods Enzymol. 104, 370-381.

APPENDIX

CONVECTION PROCESSES IN HANGING-DROP CRYSTAL GROWTH

A.1 Background

In hanging-drop protein crystal growing configurations, there are horizontal density gradients, and resulting flows, in the drop itself, in the air, and in the reservoir fluid. These motions are coupled, so that density gradients in any one of the three alone would cause motion in the other two media. On the other hand, this coupling is weak, and in practice the motions are essentially independent.

Axisymmetry is a good approximation. For definiteness, we can assume a hemispherical drop of radius a(t), and a cylindrical cell with radius b and air volume $\pi b^2 h$. The volume flux of water from drop to reservoir is $-2\pi a^2 \dot{a}$; it is diffused as vapor through the air, and diffuses into the "brine" in the reservoir. Changes in the water content of the air are negligible, so the total flux varies only with time.

A.2 Convection in the Reservoir

The water vapor flux into the brine is proportional to the excess of the partial pressure of the water vapor over the local saturation vapor pressure of the brine. Thermal effects of the condensation are negligible, since the diffusivity of heat is higher and the heat can diffuse away.

With more water vapor arriving near the axis, the brine near the axis is diluted more than the brine at the circumference of the reservoir. This establishes a convection flow in the reservoir, which tends to keep the brine concentration independent of radius. Only a very slow circulation is required to do this, particularly as convection in the air tends to keep the water vapor flux uniform over the brine surface.

A.3 Convection in the Vapor Phase

The vapor pressure in the air is highest near the drop, and lowest near the brine, so the air is lightest near the drop and heaviest near the brine. thus the convection pattern is self stabilizing. Most of the convection is in the layers beside the drop, where the water vapor spreads horizontally by convection, before diffusing down to the brine.

A.4 Convection in the Drop

The removal of the water flux from the drop increases the concentration at the drop boundary both of the protein of interest and of any secondary solutes either present as impurity or deliberately introduced to limit the evaporation. The protein has a very low diffusivity, so this increase in concentration will only slowly diffuse through the drop. The concentration variations drive both buoyancy convection and Marangoni convection in the hanging drop. The solute-rich layer on the outside of the drop will want to sink to the bottom of the drop under gravity. On the other hand, the higher concentration will lower the surface tension, driving a Marangoni circulation in the opposite direction.

A.5 Summary and Illustration

The following figure shows qualitatively the isopycnals on the left, and the streamlines of the circulation on the right. The water vapor flux from the drop to the brine causes a low-density layer in the brine, a high-density layer in the drop and density stratification and convection in the air. The drop convection is modified by surface tension variations.

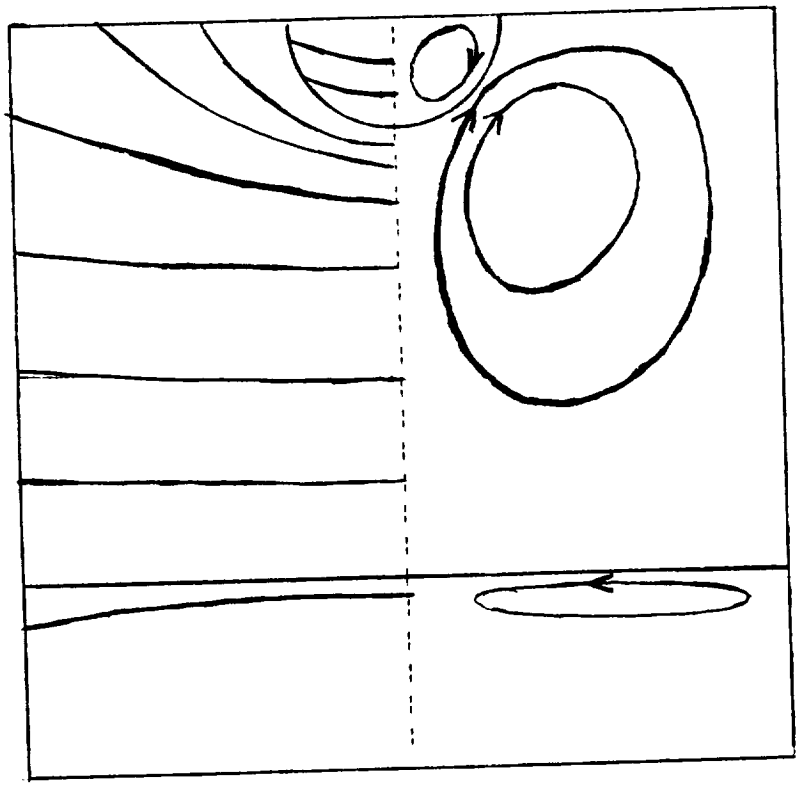

Figure 32. Convection Processes in a Hanging Drop Configuration